CHAPTER FOUR

RESULTS

**Plate 4.1. Phosphate Hill PG Stack (Cells 1 and 2) and Re-slurry Tank
Stack completed, September 2003**

4.0   RESULTS

4.1   Introduction

A number of analytical methods were carried out on a variety of PG products and its leachate in order to gain the widest possible spectrum of results. The methods were chosen to provide both the chemical and physical parameters of the PG. All of the PG samples were submitted to XRF and/or XRD analysis for major and trace elements, with SEM work being carried out on the solid phase of the samples. The slurry also underwent particle sizing, ICPMS analyses of the liquid phase and radionuclide analysis. Leachate was subjected to a variety of analyses including those for major and trace elements, both total and filterable reactive phosphorous and silica.

The sampling program has produced a wealth of results which will fully characterise the material for the first time and provide a valuable basis for future research. A summary of the results for each type of PG sampled is presented separately below and discussed fully in Section 5.

4.2   PG Slurry

Immediately upon sampling the PG slurry separated out into liquid and solid phases within the sample container. The liquid phase consists of both reused acid process water (drained from the stack and added to the HH PG filter cake in the re-slurry tank), as well as residual acids contained within the filter cake. The solid phase consists of DH PG produced after reaction of the HH filter cake with the acid process water in the re-slurry tank, with minor relict HH, quartz and other acid insolubles. Both phases were chemically analysed, the liquid *via* ICPMS and the solid with XRF and XRD, and also subjected to radionuclide analysis. Particle sizing was also carried out on the solids.

The samples were numbered PG001 to PG012 and full details of their sampling and results are contained in Appendix 1. Two sample bottles were taken on each sampling occasion, given the suffix A and B, to act as field duplicates. It should be noted that PG011 was sampled immediately after the fertilizer plants had recommenced operations after a major shut-down for repairs and upgrades. After the sample had been taken and

sent for analysis it was found that, due to incorrect settings, the phosphoric acid plant had been producing DH PG, not HH as is normally the case. As such, PG011 is presented separately in the results tables.

Table 4.1 shows the quantified mineralogy from the solid phase results. It was not possible to definitively identify the amphibole due to lack of microprobe work but, if the XRD identification of amphibole is correct, it is presumably relict material derived from the basement lower Proterozoic granitoids and metasediments during deposition of the phosphorite ore body. The mica minerals were also not identified in this study, except for one sample identified as paragonite, but have been noted as sericite and glauconite in the Beetle Creek Formation and Inca Shale (Russell and Trueman 1971) and, more recently, identified as predominantly muscovite and glauconite (Hough 2004, Mascini 2001). Both mica and amphibole were identified in 9 of 24 samples. Repeatability studies were not carried out on the samples. The SIROQUANT software does not provide precision and accuracy measurements as these are sample-dependant.

PG001-010; PG012 (%) n =22	Mean	Min.	Max.	Median	Standard Deviation
Quartz (SiO_2)	18	2	25	20	5.6
Gypsum ($CaSO_4.2H_2O$+$.0.5H_2O$)	65	39	81	66.5	10.8
Anhydrite ($CaSO_4$)	5	0	19	3	5.1
Bassanite ($CaSO_4.0.5H_2O$)	6	0	36	1	11
Mica (❖Muscovite $K_2Al_4[Si_6Al_2O_{20}](OH,F)_4$, Glauconite: $(K,Ca,Na)_{\sim1.6}(Fe^{3+},Al,Mg,Fe^{2+})_{4.0}Si_{7.3}Al_{0.7}O_{20}(OH)_4)$ Paragonite: $NaAl_2(Si_3Al)O_{10}(OH)_2$	4	2	10	4	2.4
Smectite $(0.5Ca,Na)_{0.7}(Al,Mg,Fe)_4[(Si,Al)_8O_{20}](OH)_4.nH_2O$	2	1	6	1.5	1.7
Amphibole (unidentified)	8	2	17	8	5.2
Clinoptilolite $(Na,K)_6[Al_6Si_{30}O_{72}].24H_2O$	3	1	4	3	1.3
Heulandite $(Ca,Na_2,K_2)_4[Al_8Si_{28}O_{72}].24H_2O$	4	4	4	4	
PG0011 (%) n = 2					
Quartz (SiO_2)	19	19	19	19	0
Gypsum ($CaSO_4.2H_2O$+$.0.5H_2O$)	35	26	45	35.5	13.4
Anhydrite $CaSO_4$	28	24	32	28	5.7
Bassanite ($CaSO_4.0.5H_2O$)	11	6.0	17.0	11.5	7.8
Smectite	4	3.0	6.0	4.5	2.1
Clinoptilolite	2	2.0	3.0	2.5	0.7

Table 4.1.   Average Quantified Mineralogy, PG slurry. Note: only one sample contained Heulandite. Type chemical formulae taken from Deer *et al.* 1992. *The specification of $CaSO_4.2H_2O$+*$.0.5H_2O$ is the total of standard dihydrate gypsum plus dihydrate with additional partial or complete molecules of water attached to it. ❖Type chemical formulae for the three known mica species (Hough 2004, Mascini 2001).

4.2.1 PG SLURRY LIQUID PHASE CHEMISTRY

Three physical parameters were measured in the slurry. These were % solids, pH and turbidity. A summary of the results is presented in Table 4.2 below.

PG001-010; PG012 n = 22	Mean	Minimum	Maximum	Median	Standard Deviation
% Solids	30.7	15	70	24	16.8
pH	1.39	1.15	1.55	1.43	0.11
Turbidity	125.12	2.8	590	103	155.86
PG011 n = 21					
% Solids	42.5	40	45	42.5	3.53
pH	1.38	1.37	1.39	1.38	0.014
Turbidity	52	N/A	N/A	N/A	N/A

Table 4.2. Summary of results of physical-chemical parameters measured in PG slurry (liquid phase). Note: only one turbidity measurement was available for PG011.

All measures were variable, with turbidity in particular having a standard deviation that was greater than the mean. pH was the most consistent of the measures over the sampling period.

PG001-010; PG012 (ppm) n = 22	Mean	Minimum	Maximum	Median	Standard Deviation
Al	961	565	1380	939.9	217
Ca	1958	1320	2590	1964	305
Fe	481	311	665.9	457	102
K	219	55	439	203	100
Mg	111	71	171	110	24
Mn	111	92	138	110	12
Na	699	509	968	728	121
P	7846	31	12800	7761	3059.1
S	1603	1335	2020	1490	240
Si	2179	1830	2660	2124	239
Sr	14.9	9	25	14	4
Y	27.1	10	51	30	9.9
PG011 (ppm) n = 2					
Al	1070	1060	1080	1070	14.1
Ca	1755.1	1730	1780	1755.1	35.1
Fe	1165.1	1160.1	1170	1165.1	7
K	176	172	179.1	175	5
Mg	151	150	151	150	0.6
Mn	159	159.1	159	159	0.1
Na	815	815	815	814	0.2
P	15350	15200	15500	15350	212.1
S	1990	1970	2010	1990	28
Si	2470	2460	2480	2470	14.1
Sr	11	10.9	11.9	11	0.7
Y	47.9	47	48	47.9	0.8

Table 4.3.   Summary of major element results (ICP), PG slurry (liquid phase).

Major element analyses in all samples were dominated, as expected, by Ca, S, Si and P, reflecting the dominant mineralogical suite of gypsum and quartz (and fluorosilicates) with interstitial phosphatic fluids (Table 4.1). The latter is most likely to be relict acids (H_3PO_4) and colloidal, co-precipitated complex phosphates (Ritchie *pers. comm.* 2004). Al, Na and Fe were also high. Variability was high between samples, with standard deviations for the selected species ranging from a low of 11% for Si to 39% for P. PG011 was notable for being dominated by very elevated P levels relative to the other samples. This may reflect the poor plant performance at the time of sampling, with either greater volumes of incompletely digested phosphorite, higher levels of contained phosphoric acid, or both being the cause.

PG001-010; PG012 (ppb) n = 22	Mean	Minimum	Maximum	Median	Standard Deviation
As	786	520	1140	809	155
Ba	1568	590	4270	1230	995
Cd	238	155	387	212.9	62
Co	1400	710	2290	1320	386
Cr	2556	1800	3140	2640	358
Cu	2916	176	5320	2685	982
Ga	470.9	168	1340	337	315
Nb	24	13	45	20	9
Ni	2358	1500	3880	2290	514
Pb	153	72.1	343	141	69
Rb	1135	773.9	1470	1100.1	176
Sc	834	310	2570	680	568
Sn	22	10	20	48.9	11
Th	269	132	242.9	617	110
Ti	3879.1	1121.1	3950	6800	2140
U	3311	1001	3135	5760.1	2080
V	4633	1087	4495	7580	2800
Zr	369	88	340.9	552	232
PG011 (ppb) n = 2					
As	290	260	320	290	42
Ba	1009.9	1000	1020	1009.9	14
Cd	365	360	370	365	7.1
Co	2230	2170	2290	2230	84.9
Cr	3880	3840	3920	3880	57
Cu	5840	5770	5910	5840	99
Ga	1015	1010	1020	1015	7.1
Nb	26	26	26	26	0.3
Ni	3590	3500	3680	3590	127
Pb	162.9	162	163	162.9	0.6
Rb	1540.1	1520	1560	1540.1	28
Sc	1265	1240	1290	1265	35
Sn	26	2	26	27	24
Th	795.1	21	795.1	810	780
Ti	7775	205.1	7775	7920	7630
U	7650	212.1	7650	7800	7500
V	8275	332	8275	8510	8040
Zr	875	134	875	970	780

Table 4.4. **Summary of trace element results (ICP), PG slurry (liquid phase).**

Trace elements in all samples were dominated by V, Ti and U. Cu, Cr, Co and Ba were also consistently high. The former species, along with Ba, also had standard deviations that were almost as high as the mean (ranging from 55% for Ti to 63% for U and Ba), while Cu, Cr and Co showed less variability (34%, 14% and 28% respectively). Cd content, which is of concern at other fertilizer facilities, is reasonably low at Phosphate Hill, while Pb appears to be relatively elevated (refer also to Table 5.4).

4.2.2   PG SLURRY SOLID PHASE (DIHYDRATE) CHEMISTRY

Major and trace element results for the solid phase of the slurry are presented below. These were derived *via* XRF analysis.

PG001-010; PG012 (%) n = 22	Mean	Minimum	Maximum	Median	Standard Deviation
SiO_2	22.3	13.6	30.0	22.2	5.9
TiO_2	0.0438	0.0412	0.0450	0.044	0.0017
Al_2O_3	0.59	0.385	0.761	0.59	0.08
Fe_2O_3T	0.1238	0.082	0.178	0.1239	0.08
MnO	0.0298	0.0235	0.0393	0.028	0.0075
MgO	0.1007	0.0859	0.127	0.097	0.0113
CaO	23.9	19.5	26.6	23.8	2.3
Na_2O	0.1152	0.0637	0.157	0.1188	0.0279
K_2O	0.1345	0.0887	0.172	0.1305	0.0228
P_2O_5	2.587	1.79	4.31	2.343	0.77
SO_3	30.3	24.4	36.1	30.2	3.51
F	0.5549	0.3013	1.1	0.5268	0.20
LOI	19.8	16.2	22.5	20.1	2.19
TOTAL	**100.5797**			**100.302**	
PG0011 (%) n = 2					
SiO_2	33.6	30.1	37.2	33.6	5.0
TiO_2	0.0	0.04	0.05	0.0	0.0021
Al_2O_3	0.527	0.52	0.53	0.527	0.0081
Fe_2O_3T	0.213	0.20	0.23	0.213	0.0216
MnO	0.05	0.05	0.05	0.05	0.00
MgO	0.115	0.11	0.12	0.115	0.0014
CaO	17.9	17.7	18.1	17.9	0.29
Na_2O	0.096	0.09	0.10	0.096	0.006
K_2O	0.104	0.10	0.11	0.104	0.011
P_2O_5	3.96	3.54	4.38	3.96	0.596
SO_3	21.8	21.4	22.1	21.8	0.47
F	0.367	0.2	0.5	0.367	0.23
LOI	21.22	17.7	24.7	21.22	4.94
TOTAL	**99.952**			**99.952**	

Table 4.5.   Summary of XRF major results, PG slurry (solid phase)

The solid phase chemistry of the slurry tends to reflect that of the liquid phase. CaO, SO_3, P_2O_5 and SiO_2 are the dominant species in all samples and again represent the dominant mineralogy of gypsum, quartz and phosphates (co-precipitated complexes and trace amounts of undigested phosphorite) F accounts for <1% of the total and was not identified in the liquid phase. Variability in CaO and SO_3 is moderate (9.5% and 11.5% respectively) while that in SiO_2 and P_2O_5 is much higher, 26% to 30% respectively.

PG001-010; PG012 (ppm) n = 22	Mean	Minimum	Maximum	Median	Standard Deviation
As	10.3	1	83	3.5	18.4
Ba	321.73	248	546	309	69.9
Co	8.63	3	25	5.5	6.7
Cr	21.3	16	32	21	4.89
Cu	43.4	12	148	18	44.8
Ga	3	bd	3	3	0
Mn	246.7	140	404	230	73.1
Ni	6.3	bd	28	4	7.6
Pb	18.8	11	67	14	18.1
Sc	7.82	4	10	8	1.5
Sr	363.4	327	402	364.5	20.7
Ti	179.3	143	214	181	17.6
V	17.8	10	28	17.5	4.8
Y	153.3	113	184	156	20.2
Zn	27.8	16	53	26.5	9.4
Zr	9.6	5	32	8	5.6
PG0011 (%) n = 2					
As	4.5	3	6	4.5	2.1
Ba	274.5	265	284	274.5	13.4
Co	28.5	22	35	28.5	9.2
Cr	64	35	93	64	41.0
Cu	24.5	24	25	24.5	0.7
Ga	bd	N/A	N/A	N/A	N/A
Mn	377	347	407	377	42.4
Ni	9	8	10	9	1.4
Pb	12.5	11	14	12.5	2.1
Sc	7.5	7	8	7.5	0.71
Sr	296	269	323	296	38.2
Ti	267	203	331	267	90.5
V	32	28	36	32	5.7
Y	99.5	91	108	99.5	12.0
Zn	49.5	46	53	49.5	4.9
Zr	13.5	13	14	13.5	0.71

Table 4.6.   Summary of XRF trace element results, PG slurry (solid phase)

Trace element dominance patterns within the solid phase of the slurry differ to those in the liquid phase. The only elevated elements that they share are Ti and Ba. Otherwise, the dominant species are Mn, Sr and Y. U and Cd were not found in the solid phase and Pb was moderate. Standard deviations within the dominant elements remained moderate to high, at between 6% (Sr) and 29% (Mn).

The slurry analyses confirmed that gypsum species ($CaSO_4.nH_2O$) and quartz (SiO_2) were the dominant species. Clay minerals were also not unexpected, derived from the ore body. However, the identification of amphibole was not expected and thus provided previously unknown information.

4.2.3   RELATIVE ELEMENTAL ABUNDANCE

After conversion of the results in Tables 4.3 to 4.6 (inclusive) to elemental concentrations (see page 233, Appendix 1, for details of conversion process*) a comparison of relative elemental abundance within both phases of the slurry was undertaken. The results are shown in Figures 4.1 and 4.2 below.
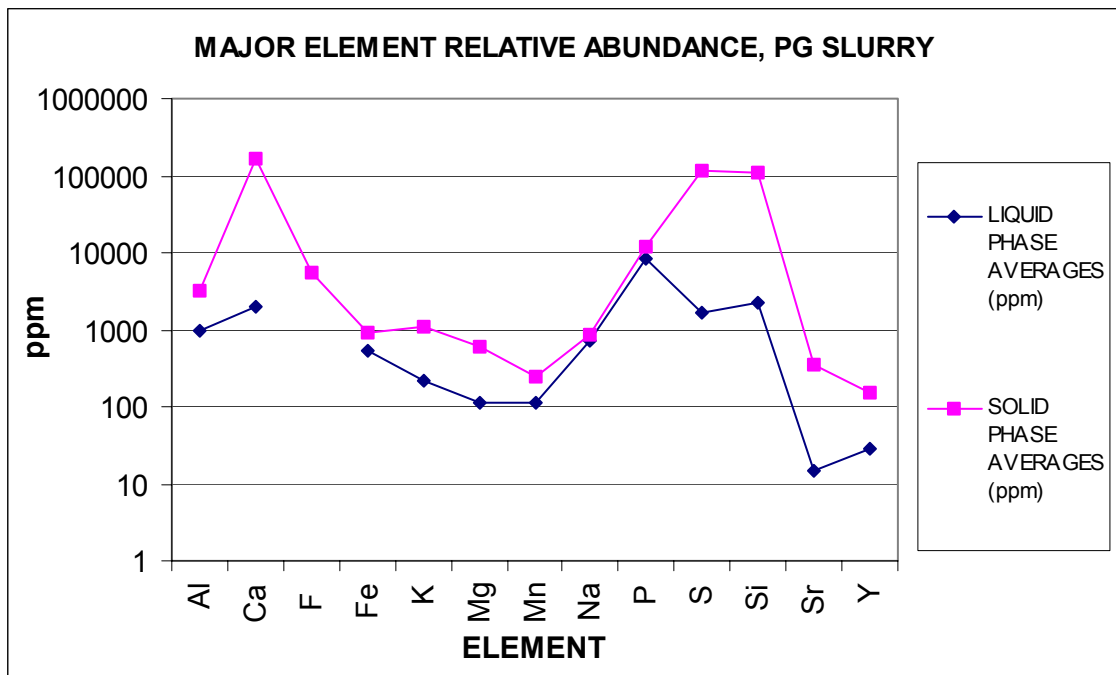
Figure 4.1   Major element relative abundance, PG slurry (ppm).   n = 24 for both phases.

All elements are found at their most abundant in the solid (PG) phase of the slurry. With the major elements occurring in both phases, Ca, S and Si most strongly favour the solid phase, reflecting the basic gypsum and quartz mineralogy. Although there appears to be little difference between abundance of P in solid and liquid phase, P would be expected to partition most strongly into the liquid phase under these highly acidic conditions, with the majority of the element present as pore-bound H_3PO_4. Internal WMCF analyses suggest that no more than 1% of the total solid mass of the HH sent to

the re-slurry tank consists of solids, primarily as co-crystallised phosphate minerals with very small amounts of unreacted phosphate rock and with the rest being in the water-soluble form. F was not analysed in the liquid phase.
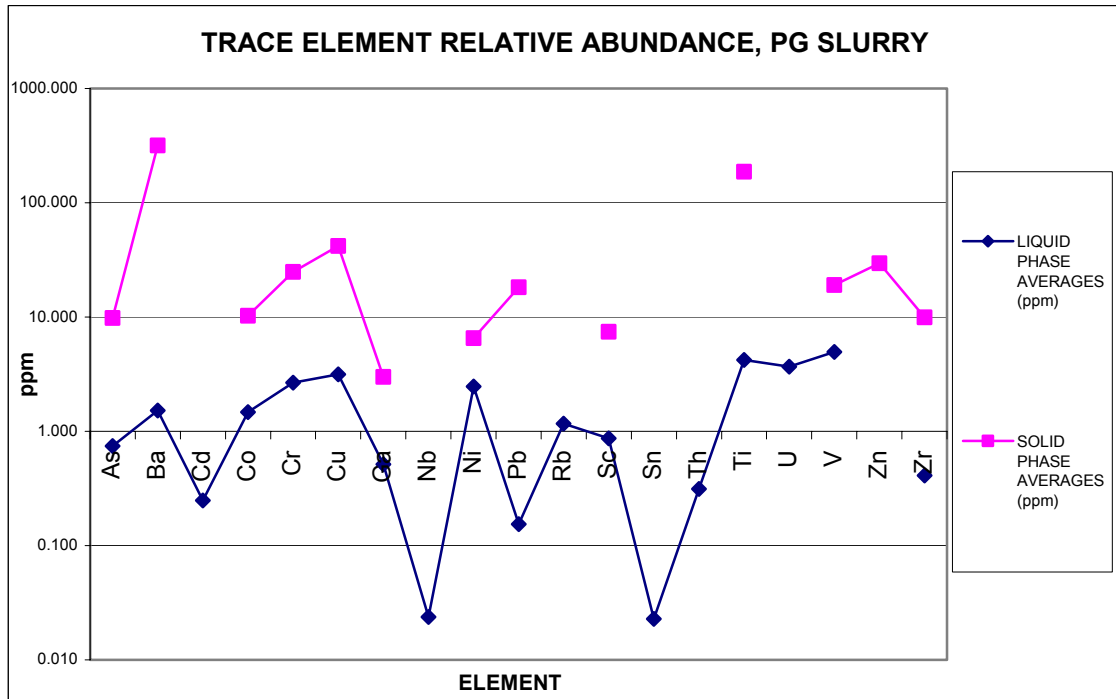
Figure 4.2   Trace element relative abundance, PG Slurry (ppm). n = 24 for both phases.

Ba and Ti were the most abundant of any element in either phase and the only ones reaching levels of >100ppm, with Ti, U and V being the most abundant in the liquid phase.. Nb, Rb, Th and U, although analysed for, were below detection in the solid phase and almost all elements occur at very low volumes (<100ppm) in both phases, with the majority of them being very close to detection limits, particularly in the liquid phase. Cd and Sn were only analysed in the liquid phase while Zn was only analysed in the solid phase. Mn, Sr and Y are included in Figure 4.1, as they appeared as major element results for the slurry liquid but as trace elements for the solid phase results.

4.2.4   PG SLURRY PARTICLE SIZING

Particle sizing of PG was undertaken using a Malvern Mastersizer-X. The complete results are in Appendix 8 and summaries shown in Table 4.7 and Figure 5.2 below.

	Minimum	Maximum	Dominant Size Fraction	>50% of total size range
Size	1.8-4.86mµ	1356.26-1646.98mµ	49.95-60.65mµ	27.89-194.5mµ
% Total	1.48%	0.08%	6.19%	54.27%

Table 4.7.   Summary of PG particle sizing results (sizes in microns). n = 24.

The dominant size fraction was between 49.95-60.65 microns, while 50% of the total fell between 27.89-194.5 microns. 80% of particles were between 4.86-236.19 microns.

4.2.5   SEASONAL VARIATION

Part of the aims of this research program was to determine whether there were any changes in the composition of the PG either from seasonal factors, from sourcing the ore from different pits (where some physical and chemical characteristics, such as ore hardness and contaminant content are known to differ) or as a result of ore blend changes. Full details of slurry analyses are contained in Appendix 1 but the sampling cycle commenced in late October 2000 and was completed the following September, covering a full cycle from hot wet season (total rainfall 570mm between October-March) to cold dry season. The stack is known to react to temperature and humidity differences during the day with HF gas exhalation increasing with increasing temperature and humidity, so sampling was generally done early in the morning to avoid being on the stack at peak exhalation times (late morning to mid-afternoon) and to get the samples onto the site flight to Townsville and thence to the analysing laboratory on the same day.

The ore that was being processed at the time was drawn from the two main pits (Galah and Brolga) and was fed into the plant as a blend, generally 80% Galah:20% Brolga (Appendix 1 page 224). However, the samples in April 2001 (PG007A and B) were a combination of 60% Galah:20% Brolga:20% off-specification ore) and in June 2001 (PG009A and B) were the result of a blend of 70% Galah:30% Brolga. 18 different ore parcels were consumed over the year, five from Brolga, 12 from Galah and the off-spec stockpile. Beneficiation (raw, uncrushed rock) and phosphoric acid (crushed and washed rock) feed P_2O_5 analyses, taken from the daily WMCF analyses and recorded in the on-site Honeywell Production Information Management System (PIMS) database,

was reasonably consistent, averaging 22.96% and ranged between 21.4% and 25.01%, inside two standard deviations of the mean (Figure 4.3). Fe_2O_3 and Al_2O_3 grades were similarly consistent (Appendix 1 pages 240 and 241). PG010A/B (4.7.01) was the final sample taken before a major, scheduled, plant maintenance shutdown and PG011A/B (27.8.01) was the first sample taken after plant start-up and was the sample found to be the result of the plant producing DH instead of HH.
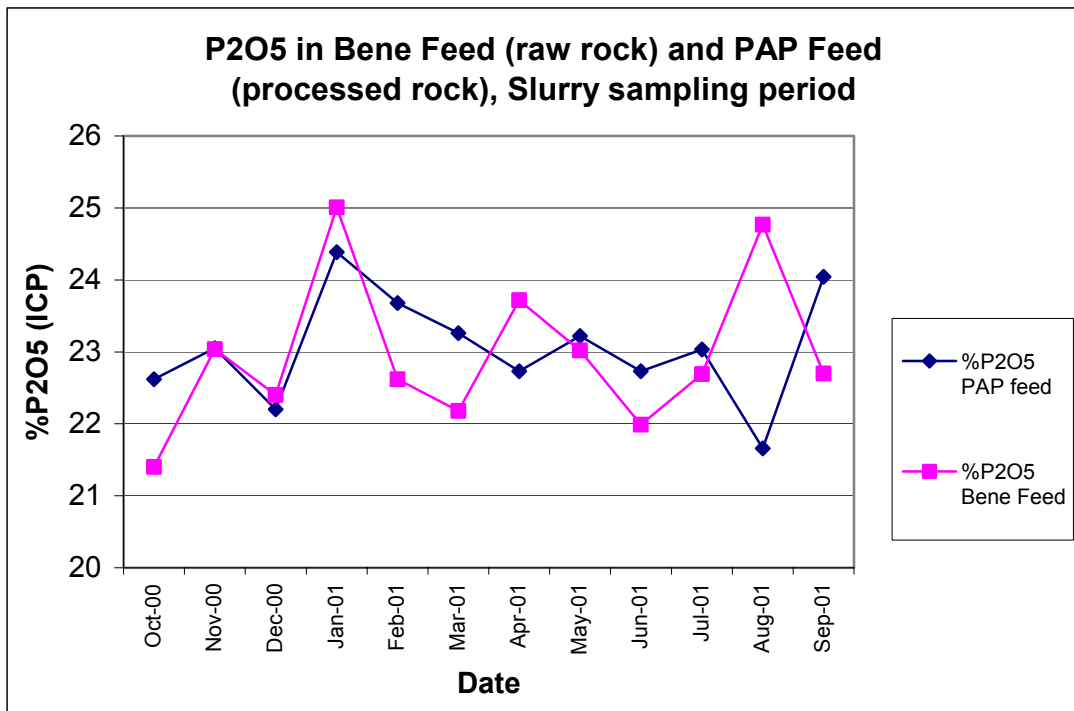

Figure 4.3. **Beneficiation and phosphoric acid plant feed grades at PG slurry sampling dates. Pink = raw rock into beneficiation plant (mean of 3 samples taken over 24 hours on each sampling date); Blue = crushed and washed rock filter cake into PAP reactor 1A (mean of 7 samples over 24 hours on each sampling date). ICP data from WMCF PIMS database.**

Statistics for the quantified mineralogy of the PG slurry are presented in Table 4.3 above and graphs of the major solid constituents are presented in Figures 4.4 and 4.5 below.
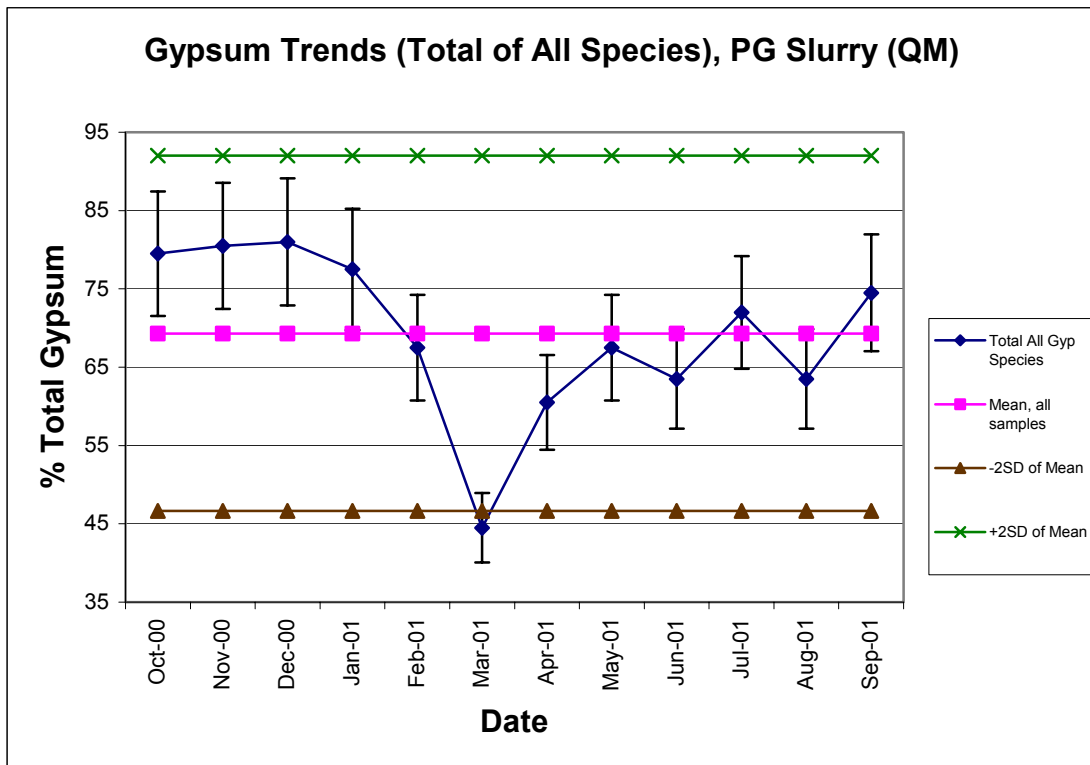
Figure 4.4. Quantified mineralogy trends (all gypsum species) over 12 month slurry sampling period. n = 24. Blue is the total of all gypsum species in a given sample; pink is the mean of all samples over the 12 month period; green and brown = +/- two standard deviations of the mean.
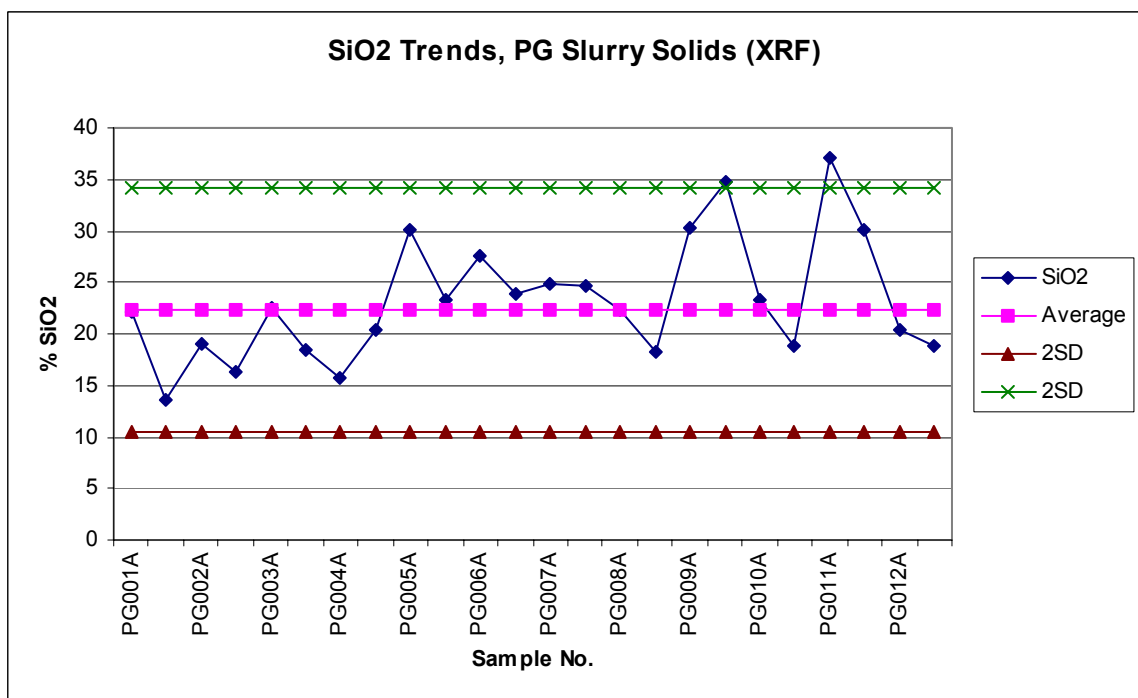
Figure 4.5. XRF trends for SiO$_2$ over 12 month slurry (solids) sampling period. n = 24 Blue = total SiO$_2$ in each sample. Pink is the mean of all samples over the 12 month period; green and brown = +/- two standard deviations of the mean.

Although no seasonal trends are evident, there is a clear downwards trend in total gypsum content (Figures 4.4 and 5.4) and a corresponding upwards trend in SiO_2 content (Figure 4.5) over the 12 months. SO_3 and trace elements such as F (which is liberated into the PG during acidulation) and Sr (Appendix 1 page 239) also show downward trends while P_2O_5 increases over the period (Figure 5.4). Together, these results suggest that over the 12 month sampling period the relative gypsum content of the slurry was decreasing while the relative quartz (probably including soluble silicates such as fluorosilicic acid) and phosphate (most probably in the form of phosphoric acid and co-precipitated P_2O_5 with minor unreacted phosphorite) content were increasing. ICP results from the slurry liquid over the period indicate that both P and S were rising while Ca was falling (Appendix 1 page 227). The most likely explanation for this, as discussed in Anon 1999, is that the growing instability in the plant during the months leading to the shutdown was not only causing increased loss of H_3PO_4 to the gypsum stack through poor filtering but was also causing co-crystallisation of P_2O_5 with the HH through isomorphic substitution of HPO_4^- for SO_4^-. Poor performance may have also led to greater amounts of H_2SO_4 being sent to the stack in the waste process fluids used to re-slurry the HH.

An examination of P_2O_5 grades in both the raw rock entering the beneficiation plant and the washed, crushed rock filter cake fed into the main reactor of the phosphoric acid plant (PAP) (Figure 4.3) shows that the feed grade trend for these elements was flat over the same period. This suggests that the cause of the rise in P_2O_5 within the PG was related to problems within the PAP and not a result of increased feed grade, and probably reflects poor recoveries of phosphoric acid from the PG filter cake (refer section 5 below, Appendix 1 pages 240 and 241 and Appendix 2 pages 248-249; 252-253; 256-257; 260-261; 264-265; 268-269; 272-273; 276-277; 280-281; 284-285; 288-289 and 292-293). There may also be some influence on the levels of P_2O_5 from increased relict ore particles (due to lack of completion of the acidulation process) as the overall gypsum content fell (Figure 4.4) while the total content of solids in the slurry was rising over the same period (Figure 4.6).
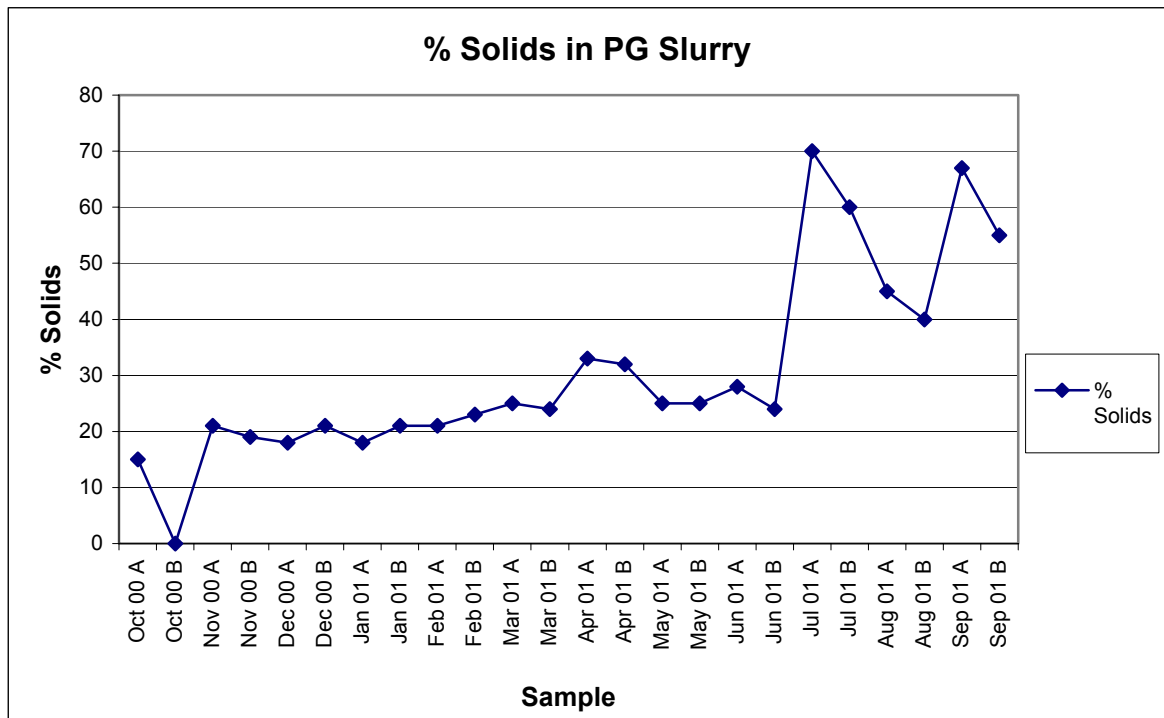
Figure 4.6. **Solids content of slurry samples. n = 24**

Poor PAP performance can also be seen when comparing the levels of individual gypsum species within the slurry over the period (Figures 4.7 and 5.4). This is particularly noticeable in August 2001 where a spike in anhydrite is reflected by a concurrent fall in DH. This sample was taken immediately after the shutdown, in the period of slow re-starting of the plant, when the PAP was known to be making something other than HH due to incorrect settings in the reactors. At the time it was believed to be DH but the results in Figure 4.7 suggest it was a mix of anhydrite (caused by too high temperatures in the reactors) and HH. The HH spike in the same sample may also be the result of partial rehydration of some of the anhydrite in the original sample over the period between sampling and analysing or mis-identification of the individual species in the XRD results.

Gypsum Species in Slurry (XRD)
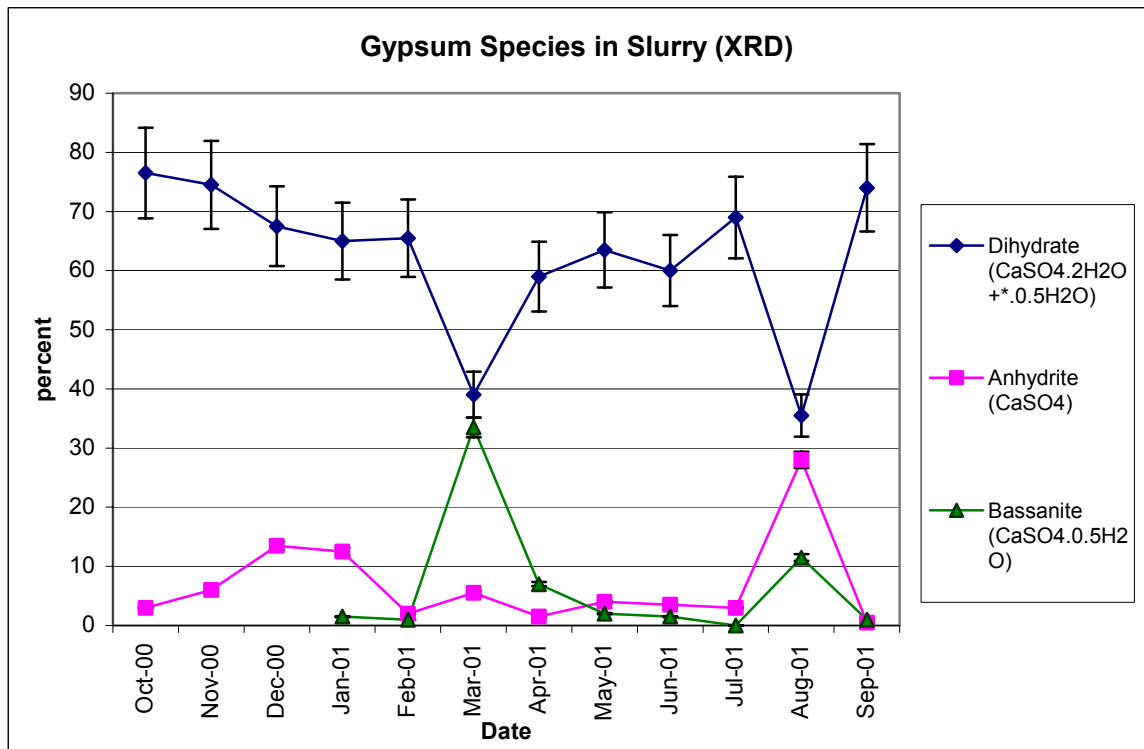
Figure 4.7   Comparison of gypsum species (quantitative mineralogy) in slurry over the 12 month sampling period.

There is also a notable drop in DH levels, mirrored by an increase in bassanite (HH), in the March 2001 samples. The cause is uncertain but may relate to the breakdowns occurring in the plant at the time or inadequate mixing in the re-slurry tank reducing the amount of HH→DH conversion taking place before the slurry was piped to the stack. It is also quite possible that it is a simple mis-identification of the gypsum species by the quantitative XRD.

4.2.6   HEAVY METALS

Charts for Pb (solid and liquid phase) and Cd (liquid phase only) are presented below.
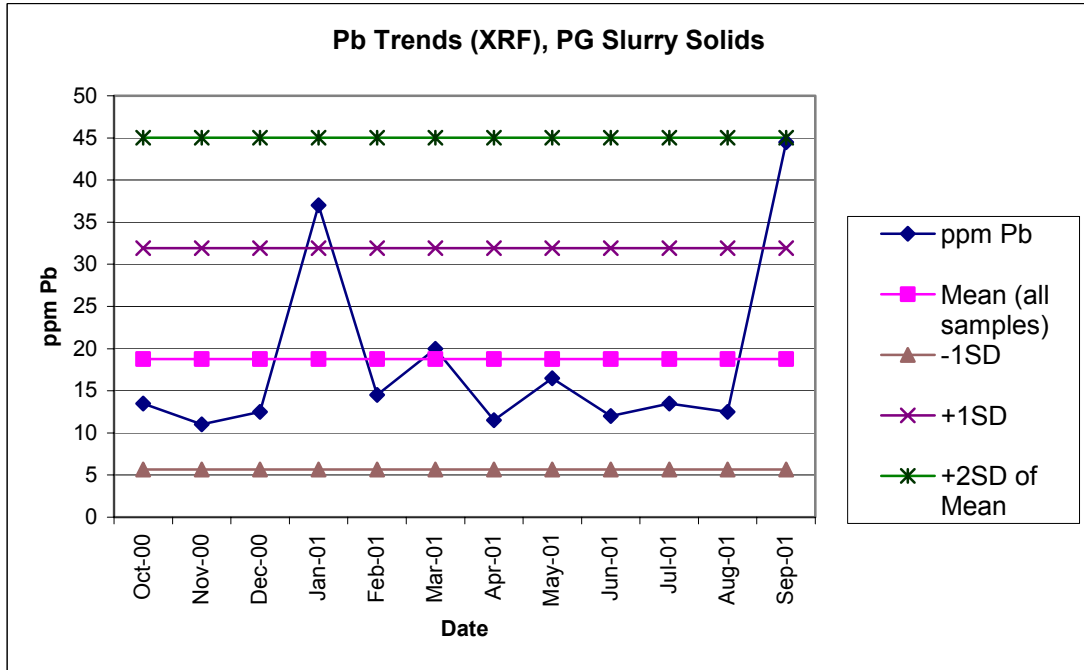
Figure 4.8.   XRF solid phase trends for Pb over 12 month slurry sampling period.   n = 24.   Blue = ppm Pb in monthly sample;   pink = mean of all samples over 12 month sampling period;   purple and puce = +/- 1 standard deviation of the mean;   green = + 2 standard deviations of the mean.
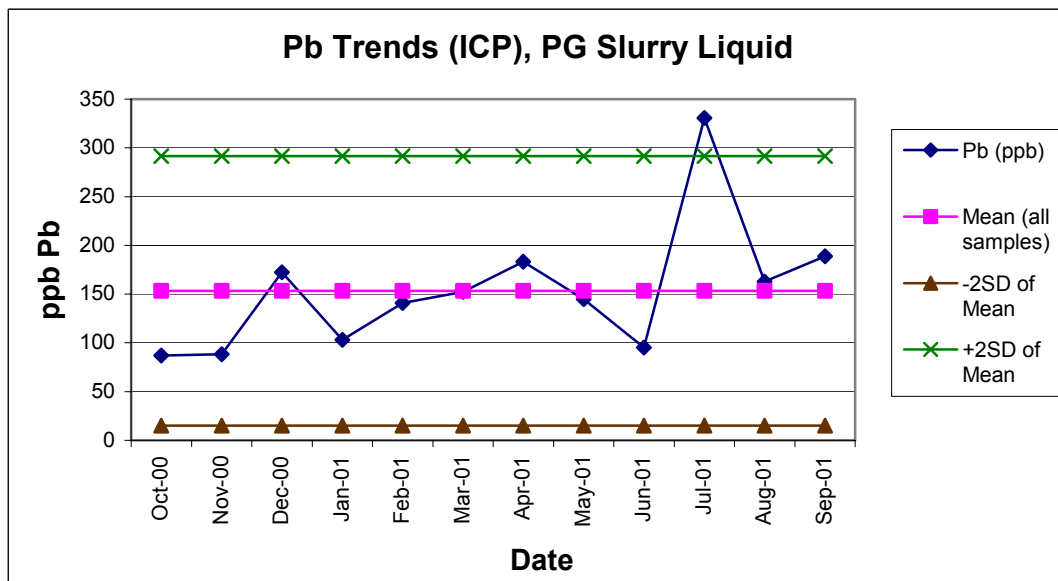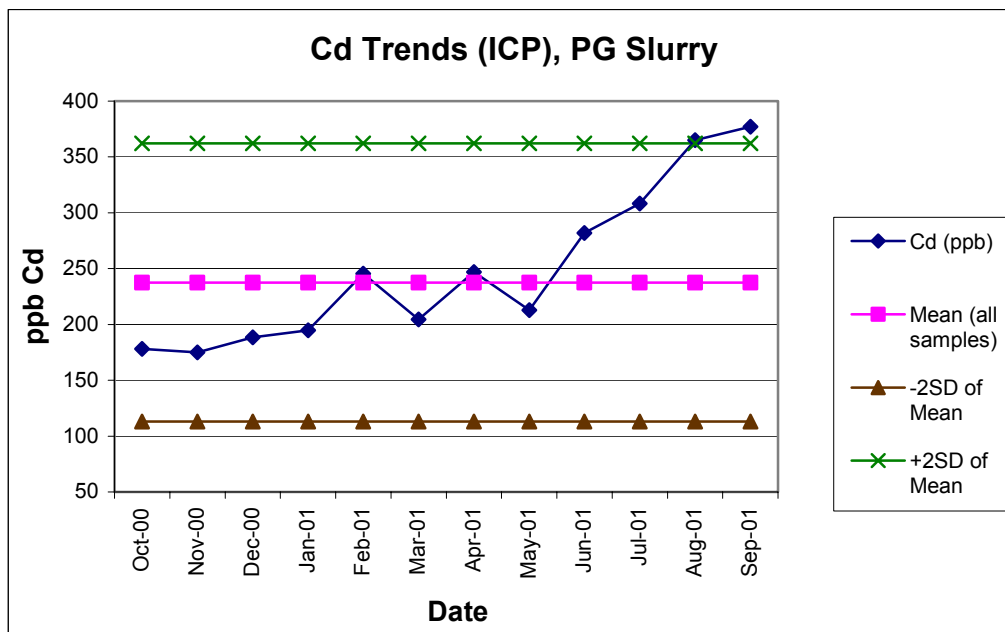

Figure 4.9   ICP liquid phase trends for Pb over 12 month slurry sampling period.   n = 24.   Blue = Pb in monthly sample;   pink = mean of all samples over 12 month sampling period;   green and brown = +/- 2 standard deviations of the mean.

Figure 4.10 ICP liquid phase trends for Cd over 12 month slurry sampling period. n = 24. Blue = Cd in monthly sample; pink = mean of all samples over 12 month sampling period; green and brown = +/- 2 standard deviations of the mean.

ICP analysis of the slurry suggests a slight increase in both Pb and Cd over the 12 month sampling period. This may also reflect poorer plant performance as discussed elsewhere as Pb tends to partition into the phosphoric acid rather than into the PG (Burnett *et al.* 1995), suggesting that recoveries of phosphoric acid were falling in the plant and thus the amount of acid arriving at the stack with the gypsum was increasing. The increase in Cd may also reflect a drop in the solid compared to liquid components in the slurry as a result of poor recoveries in the PAP as Cd levels are often high in the acid process water used in acidulation (Heerings and Zeldenrust 2000, Rutherford *et al.* 1994). pH in the slurry liquid fell slightly over the period June-September 2001 (Figure 4.11), probably a result of increased acids in the gypsum circuit, which may also have contributed to the increases in Pb and Cd in the latter part of the sampling period.
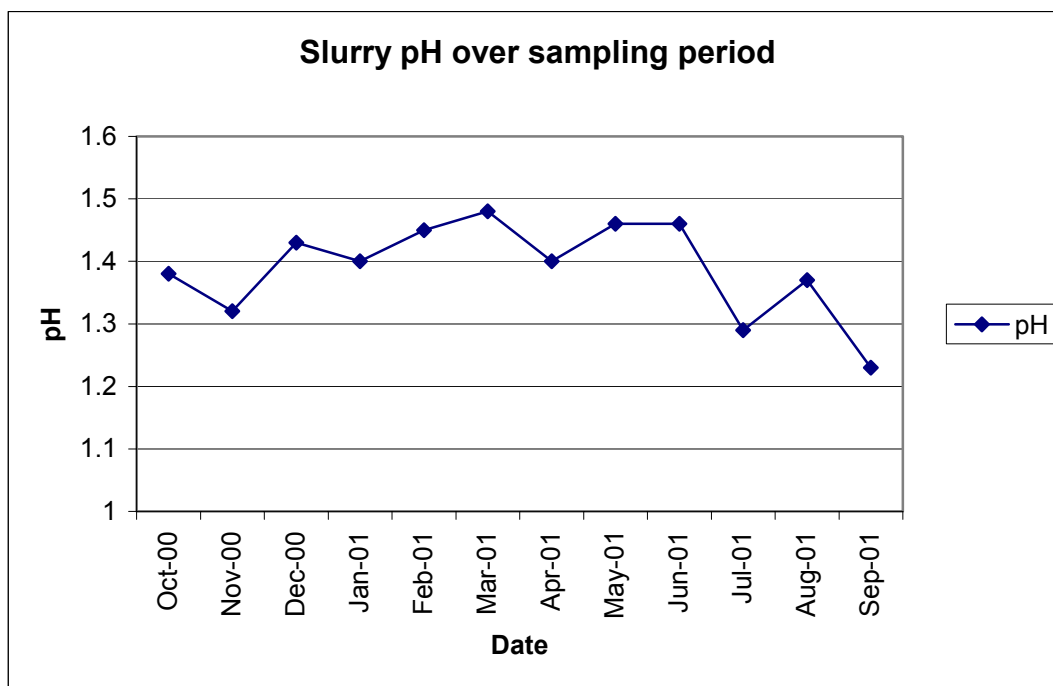
Figure 4.11 pH trends (averaged for each month) in PG slurry over 12 month sampling period. n = 24.

4.3 Dihydrate PG

DH PG was sampled from both the main stack and the emergency dumping stack on two occasions in relation to the preparation of the dissolution columns. For the original field columns, 80kg of material was removed from an area of the stack that had recently been deposited and a further 80kg removed from the emergency stack where it was at least seven months old. This was to compare any differences that may result from using newly deposited, wetter material or older, dryer PG as backfill.

For the laboratory columns new areas had to be sampled, as the previous ones were either unreachable or destroyed. In this case, approximately 1kg of newly-deposited PG was taken from a similar area, older (3-5 months) material from lower down the stack and HH from directly off the outfall of the conveyor belt. This was done for the same reasons, to compare any differences that might occur not only between DH and HH but between older, dryer and fresh, wet DH.

All samples were analysed by both XRF, XRD and SEM and summaries of the results are tabled below in Tables 4.8 to 4.10 inclusive.

4.3.1   DIHYDRATE PG XRF RESULTS

Major Elements (wt%) n = 4	Mean	Minimum	Maximum	Median	Standard Deviation
SiO_2	35.6	14.1	61.3	33.5	19.7
TiO_2	0.035	0.02	0.05	0.036	0.0126
Al_2O_3	0.536	0.31	0.69	0.573	0.1708
Fe_2O_3T	0.126	0.11	0.24	0.117	0.086
MnO	0.033	0.01	0.06	0.032	0.0195
MgO	0.078	0.04	0.11	0.083	0.0335
CaO	17.1	11.1	22.1	17.5	5.03
Na_2O	0.098	0.08	0.11	0.100	0.0134
K_2O	0.097	0.06	0.12	0.103	0.0279
P_2O_5	2.65	2.2	3.78	2.305	0.7563
SO_3	27.4	12.2	41.59	27.97	12.07
F	0.5	0.4	0.6	0.5	0.08
LOI	15.7	11.0	20.6	15.7	4.8
TOTAL	**99.953**			**98.519**	

Table 4.8.   Summary of major element results, DH PG.

Major elements are, as expected, dominated by Ca, S, Si and P, reflecting the primary gypsum and quartz mineralogy (Table 4.10) with contained acids, co-precipitated phosphates and minor unreacted phosphorite. F again measures <1%. The results mirror those from the solid component of the slurry, suggesting that there is little change in mineral chemistry between the gypsum product undergoing HH $\rightarrow$ DH conversion in the slurry and that which has been drying in the stack over any given period. Variabilities are again high in the dominant species, with CaO and P_2O_5 at 29%, SO_3 at 44% and SiO_2 at 55%.

Trace element (ppm) n = 4	Mean	Minimum	Maximum	Median	Standard Deviation
As	7.5	3	12	7.5	3.697
Ba	317.5	250	428	296	85.13
Co	8.25	4	11	9	3.09
Cr	41.5	28	64	37	16.34
Cu	22	14	25	24.5	5.35
Ga	3	bd	3	3	
Mn	409.25	284	525	414	117.3
Ni	7.25	3	11	7.5	3.5
Pb	10.75	9	15	9.5	2.87
Sc	6	4	9	5.5	2.6
Sr	291.5	185	354	310.5	82.747
Ti	204.5	166	275	188.5	48.47
V	23	16	34	21	7.75
Y	119	71	199	103	55.91
Zn	40.75	27	48	44	9.39
Zr	17.75	1	48	11	21.282

Table 4.9.   Summary of trace element results, DH PG.

Again reflecting the chemistry of the solid components of the slurry, crystalline PG shows Ba, Mn, Sr, Ti and Y as being the dominant trace elements. Variability is again high, as shown by a range of standard deviations for the named elements from 24% for Ti to 47% for Y.

Mineralogy (vol%) n = 4	Mean	Minimum	Maximum	Median	Standard Deviation
Quartz (SiO_2)	22.95	16.3	29.0	23.25	6.25
*Gypsum $CaSO_4.2H_2O+*.0.5H_2O$	54.28	26.0	82.9	54.1	23.29
Anhydrite ($CaSO_4$)	11.25	1.0	32.0	6.0	14.06
Bassanite ($CaSO_4.0.5H_2O$)	9.25	0.0	17.0	10.0	7.18
Clinoptilolite	1.5	1.0	2.0	1.5	0.71
Thaumasite	1.0	1.0	1.0	1.0	0
Sepiolite	0.5	0.0	1.0	0.5	0.71
Expanding Clays	1.0			1.0	

Table 4.10.   Summary of average quantified mineralogy, DH PG.   *The specification of $CaSO_4.2H_2O+*.0.5H_2O$ is the total of standard dihydrate gypsum plus dihydrate with additional partial or complete molecules of water attached to it.

XRD quantitative mineralogy identifies gypsum and quartz as comprising over 90% of the PG. It does not identify any phosphate minerals but the quartz is phosphatised

(Russell & Trueman 1971, Rogers & Crase 1979, Plates 4.8 and 4.10) and it is possible that some substitution of HPO_4^- for SO_4^- in the gypsum lattice has also occurred (Anon 1999). Phosphoric acid may also be a contributor to the P_2O_5 levels as recoveries of acid through filtration occurred at an average of 89% during the sampling period (Figure 5.4) with the remaining 11% being lost to the gypsum stack as a result of inefficient washing of the gypsum filter cake in the PAP. Other minerals that the XRD has failed to identify in these samples include the chromium-iron-managanese species observed during the SEM examination (see Section 4.3.2).

Like the solid component of the slurry, the DH PG analyses show ~75% of the total volume is taken up by gypsum species. Quartz was elevated but clays were reduced. Mica and amphibole were not identified in the DH samples. Thaumasite, a member of the ettringite group, was identified in the crystalline samples but not in the slurry.

4.3.2 DIHYDRATE PG SEM RESULTS

The primary phase identified comprised calcium-sulphur with intermixed silicon, the latter both as fine grains within the gypsum and as larger discrete grains (Plates 4.2-4.5, Figures 4.12 and 4.13). A rare chromium-iron phase was also identified as fine (2-10 microns) particles (Plate 4.3 and Figure 4.14) as were more common iron or iron-manganese-bearing and calcium-phosphate phases. The former may be chromite, which does rarely occur in the ore (Hough 2003 *pers. comm.)* or may be derived from the milling process. The metal ions are initially sourced from the iron hydroxide and pyrolusite gangue minerals in the ore which have precipitated as complex phosphate and/or oxide species during evaporation of the acidic process water (Ritchie *pers. comm*. 2004). It is also possible that the calcium-phosphate phase may be hydoxy-apatite (Ca5(PO4)₃OH that has precipitated during a reaction between the gypsum and the relict acids (Deer *et al.* 1992) or the result of substitution of HPO_4^- for SO_4^- in the PAP during the acidulation process (Anon 1999). A single grain of barium sulphate was identified in one sample.

Both the aged and the freshly deposited PG displayed a morphology of clusters of tabular PG crystals commonly 50 microns across with the individual crystals generally being less than 25 microns across (Plates 4.2, 4.4 and 4.5). Included in the clusters were

fine grains of quartz, the chromium-iron phase and a phosphorous phase (co-precipitate or relict apatite). Individual quartz grains were up to 500 microns in size, flat and angular (Plate 4.4). Full SEM results are contained within Appendix 9.
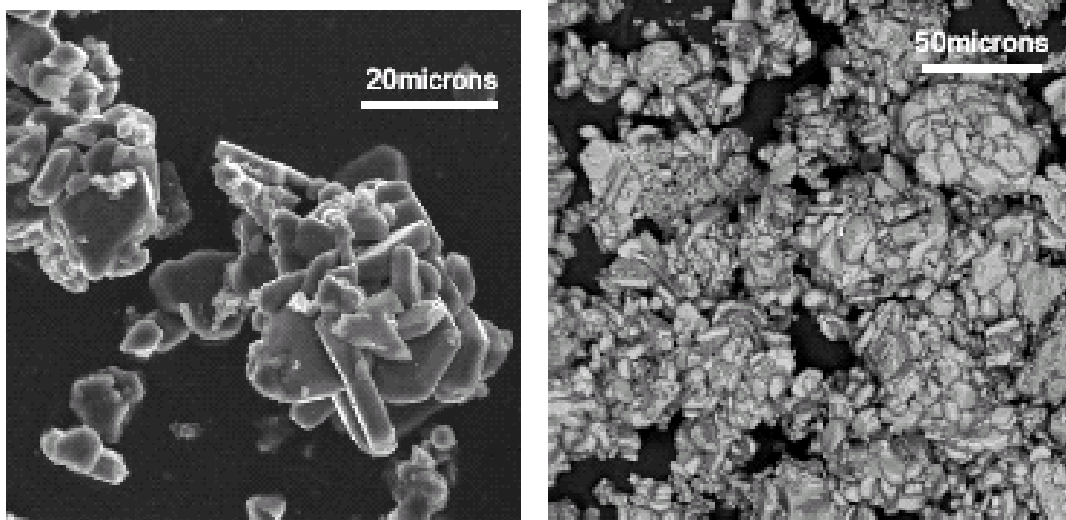

Plate 4.2. (Left) Secondary electron image of typical DH PG morphology; (right) Backscatter electron image of DH PG which shows very little variation in the average chemistry of the grains (freshly deposited DH sampled from top of stack)
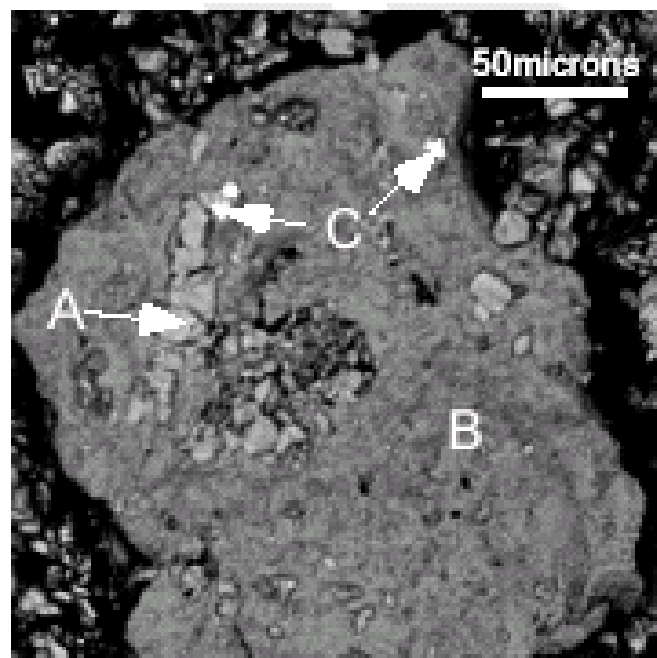

Plate 4.3. Backscatter electron image of large quartz grain (B – dark grey) with gypsum (A – mid grey) and Cr-Fe grains (C - white).
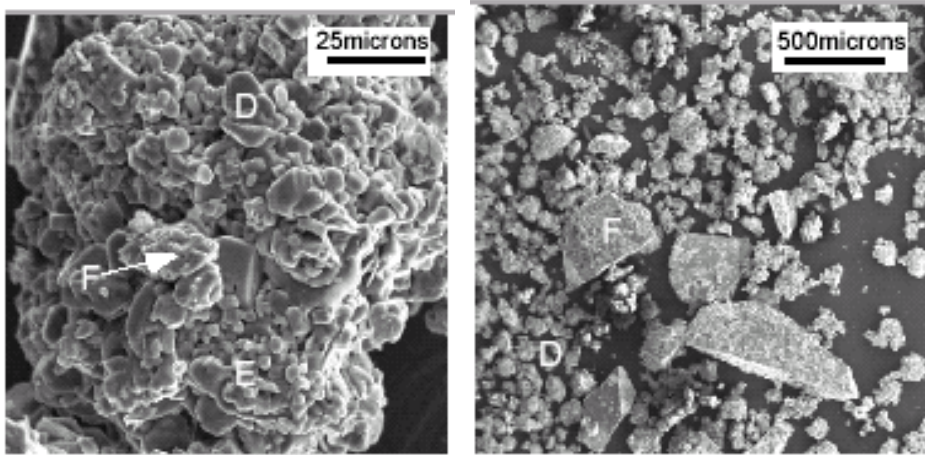
Plate 4.4. (Left) Secondary electron image of DH PG cluster containing angular quartz grains (F), fine gypsum+phosphorous+quartz (E) and bulk gypsum (D) and (Right) large angular quartz clasts (F) with matrix gypsum (D) (approximately 6-months old DH sampled from within the stack).

THIS IMAGE HAS BEEN REMOVED DUE TO COPYRIGHT RESTRICTIONS

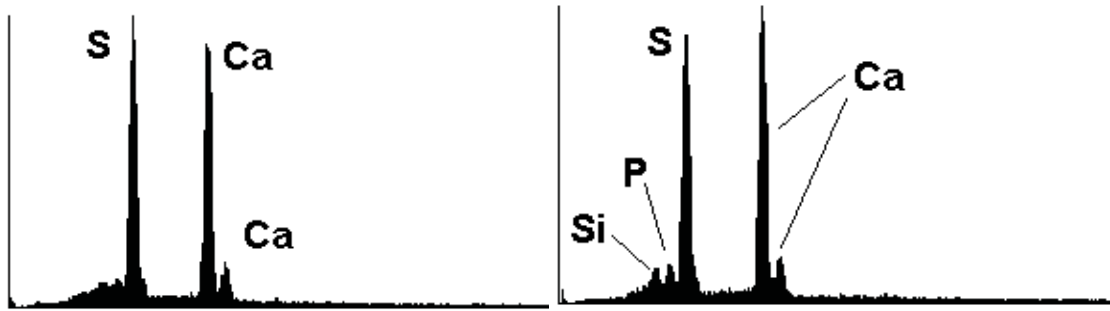**Plate 4.5. SEM image of DH PG from Ardaman (2000). Field of view 15 microns.**

Figure 4.12. Energy dispersive spectra examples – bulk of sample (DH).

Figure 4.13 Energy dispersive spectra – quartz grains.
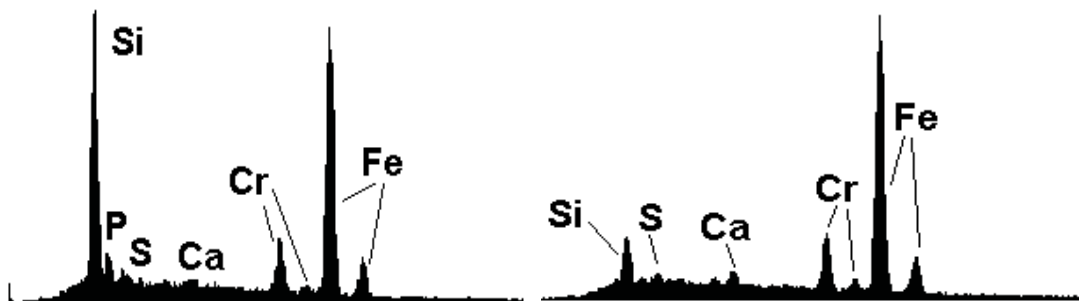
Figure 4.14 Energy dispersive spectra examples – Cr-Fe grains.

4.3.3   CORRELATION COEFFICIENTS

Correlation coefficient charts for major and trace elements for crystalline PG have been prepared and are displayed below.

	Si	Ti	Al	Fe	Mn	Mg	Ca	Na	K	P	S	F	Sc	Ba	Ti	V	Cr	Co	Ni	Cu	Zn	As	Pb	Sr	Y	Zr
Si	1																									
Ti	0.30555	1																								
Al	0.39250	0.67936	1																							
Fe	0.51649	0.65177	0.47803	1																						
Mn	0.57930	0.63533	0.49832	0.90000	1																					
Mg	0.24994	0.86516	0.73455	0.74472	0.74005	1																				
Ca	-0.81144	0.14347	-0.01020	-0.36098	-0.41603	0.11421	1																			
Na	0.10140	0.19877	0.70548	0.11072	0.26661	0.43369	0.05898	1																		
K	0.14289	0.66863	0.86940	0.44798	0.43052	0.78126	0.25590	0.70980	1																	
P	0.13343	-0.09628	0.08444	0.49450	0.50542	0.30168	-0.27391	0.35818	0.16492	1																
S	-0.86509	-0.44138	-0.43371	-0.68872	-0.75669	-0.44609	0.78305	-0.11772	-0.19981	-0.20258	1															
F	-0.28810	-0.45380	0.06714	-0.10081	-0.08136	-0.22477	0.21516	0.08798	0.16096	-0.12916	0.25063	1														
Sc	-0.10483	0.43373	0.35716	0.28435	0.28007	0.43312	0.41053	0.14264	0.43291	-0.00150	0.09590	0.28441	1													
Ba	0.31900	0.38572	0.15458	0.21683	0.33632	0.32637	-0.08816	0.04529	0.28277	-0.12306	-0.37277	-0.22351	-0.07278	1												
Ti	0.54740	0.18568	0.01944	0.31015	0.34719	0.11385	-0.53371	-0.13221	-0.14561	0.06337	-0.63702	-0.64781	-0.22907	0.27318	1											
V	0.27481	-0.23671	-0.10708	0.25109	0.35346	-0.01095	-0.42059	0.08297	-0.13331	0.68751	-0.21245	-0.27580	-0.15526	-0.14401	0.30167	1										
Cr	0.55530	-0.33880	-0.19106	0.07769	0.15148	-0.25987	-0.65328	-0.08699	-0.33962	0.34918	-0.34736	-0.36999	-0.19815	-0.24213	0.47721	0.66884	1									
Co	0.37675	-0.02038	0.10331	0.05312	0.18027	0.14247	-0.22280	0.32035	0.07329	0.42183	-0.25135	-0.46868	-0.08740	0.15247	0.36867	0.38094	0.46301	1								
Ni	0.16584	-0.26128	-0.14425	-0.10418	-0.11111	-0.15917	-0.16804	-0.13411	-0.11299	0.07766	0.03531	0.02179	0.05789	-0.18246	-0.09268	0.21999	0.53786	0.16920	1							
Cu	-0.00401	0.05840	0.17371	-0.08759	0.09920	0.19836	0.12793	0.41155	0.30406	0.24408	0.01436	-0.33113	-0.07680	0.46789	0.01289	0.29939	-0.02965	0.38053	0.11510	1						
Zn	-0.00048	-0.39783	-0.40350	0.20015	0.19142	-0.17960	-0.31511	-0.32395	-0.41732	0.55481	-0.05082	-0.06410	-0.01833	-0.25217	0.12522	0.63752	0.47561	-0.08310	0.28856	-0.02946	1					
As	0.00839	-0.16060	0.05494	-0.14449	-0.01848	-0.08660	-0.07641	0.22893	0.08854	0.09968	-0.04892	-0.25889	-0.18342	0.16346	0.07794	0.32606	0.14570	0.10499	0.26546	0.77143	0.14338	1				
Pb	-0.32162	0.19456	0.27425	0.03804	0.06091	0.31089	0.41367	0.26766	0.40450	0.12317	0.18346	-0.00946	0.23410	0.13818	-0.25821	0.08186	-0.31392	-0.13329	0.11633	0.70048	0.07728	0.67693	1			
Sr	-0.81593	-0.01466	-0.15333	-0.46004	-0.52016	-0.04715	0.93959	-0.05171	0.08972	-0.26107	0.83699	0.26504	0.32313	-0.18033	-0.60007	-0.35615	-0.60885	-0.17865	-0.14459	0.08322	-0.24524	-0.10690	0.33364	1		
Y	-0.60069	0.22121	0.26777	-0.15309	-0.20047	0.18914	0.78946	0.13989	0.35065	-0.24113	0.59232	0.51613	0.51740	-0.27549	-0.68326	-0.32291	-0.59674	-0.45506	-0.14764	-0.04615	-0.17555	-0.09988	0.42616	0.76431	1	
Zr	0.71169	0.70947	0.55698	0.66004	0.60065	0.58147	-0.37461	-0.00971	0.39382	-0.17474	-0.72721	0.00593	0.26282	0.30045	0.31220	-0.14836	0.06811	-0.01781	0.06418	-0.24847	-0.23830	-0.23600	-0.17707	-0.43719	-0.12009	1

Table 4.11   Correlation coefficients for PG slurry solids – all elements.

The strong correlation between Ca and S reflects the primary mineralogy of the PG. That between Ca and Sr may be derived from primary Sr substitution of Ca in phosphorite with a similar occurrence in gypsum, as could the correlation between Ca and Y. The correlations between Fe, Mn, V, Zn and P may reflect the precipitation of complex iron-phosphate hydroxides that are known to occur in wet gypsum pond systems (an example is the species identified in Kennedy *et al.* 1991, which was given the chemical formula $Fe_3(NH_4,K,H)H_8(PO_4)_6.6H_2O$). P to V correlations are possibly the result of substitution in apatite of P^{5+} with V^{5+} in PO_4^{3-} and VO_4^{3-}. Other correlations may also reflect sources in the primary ore mineralogy, such as Ti to Al and Mg, Al to Mg and K (micas) and they, along with correlations between Zr/Fe/Mn/Si and are possibly related to the formation of complex aluminosilicates and/or silicates. Other correlations may relate to species produced during the acidulation process, such as the alkali fluorosilicates that creates scale problems within the plant and crystallise out of the still water in areas such as the return surge ditch, reflected in the strong correlation between Na and K.

4.4   Hemihydrate PG

Due to the necessary change of plans for the leaching program mentioned in Section 3.4 above only one sample of HH PG was taken and analysed.

4.4.1   HEMIHYDRATE PG XRF RESULTS

Major Elements	wt.%
SiO_2	21.1
TiO_2	0.03
Al_2O_3	0.37
Fe_2O_3T	0.08
MnO	0.02
MgO	0.03
CaO	20.04
Na_2O	0.11
K_2O	0.08
P_2O_5	2.16
SO_3	40.17
LOI	15.2
Total:	**99.45**

Table 4.12.   Major elements, HH PG (n = 1)

The results for major analyses of HH are little different to those from the DH. CaO, SO_3, SiO_2 and P_2O_5 are again the dominant phases. However, on this occasion no F was detected.

Trace element	ppm
As	3
Ba	329
Co	7
Cr	56
Cu	21
Ga	bd
Mn	139
Ni	4
Pb	12
Sc	9
Sr	348
Ti	193
V	18
Y	152
Zn	27
Zr	8

Table 4.13.   Trace elements, HH PG (n = 1).

Again like the DH, trace elements in HH were dominated by Ba, Mn, Sr, Ti and Y, at very similar levels. The quanitified mineralogy (Table 4.14) identifies higher levels of HH and lower levels of other gypsum species. Quartz content in this particular sample was higher than average for DH.

Mineralogy (%)	Mean
Quartz (SiO_2)	32.0
*Gypsum ($CaSO_4.2H_2O+*.0.5H_2O$)	43.0
Anhydrite ($CaSO_4$)	1.0
Bassanite ($CaSO_4.0.5H_2O$)	25.0

Table 4.14.   Quantified   mineralogy,   HH   PG.   *The   specification   of $CaSO_4.2H_2O+*.0.5H_2O$ is the total of standard dihydrate gypsum plus dihydrate with additional partial or complete molecules of water attached to it (n = 1).

4.4.2 HEMIHYDRATE PG SEM RESULTS

The primary phase identified consisted of (like the DH) calcium-sulphur with intermixed silicon, the latter both as fine grains within the gypsum and as larger discrete grains. A rare chromium-iron phase was also identified in the HH as fine (2-10 microns) particles (Plate 4.6). The HH, like the DH, displayed a morphology of clusters of tabular PG crystals but these were much smaller than in the DH, being a maximum of 25 microns across and often significantly smaller (Plate 4.7). The individual crystals appear to be less than 5 microns across in most cases. Also included in the clusters were fine grained particles of quartz, the chromium-iron phase and a Ca-P phase that is either a co-precipitate or primary apatite. Individual flat and angular quartz grains were more than 25 microns in size.
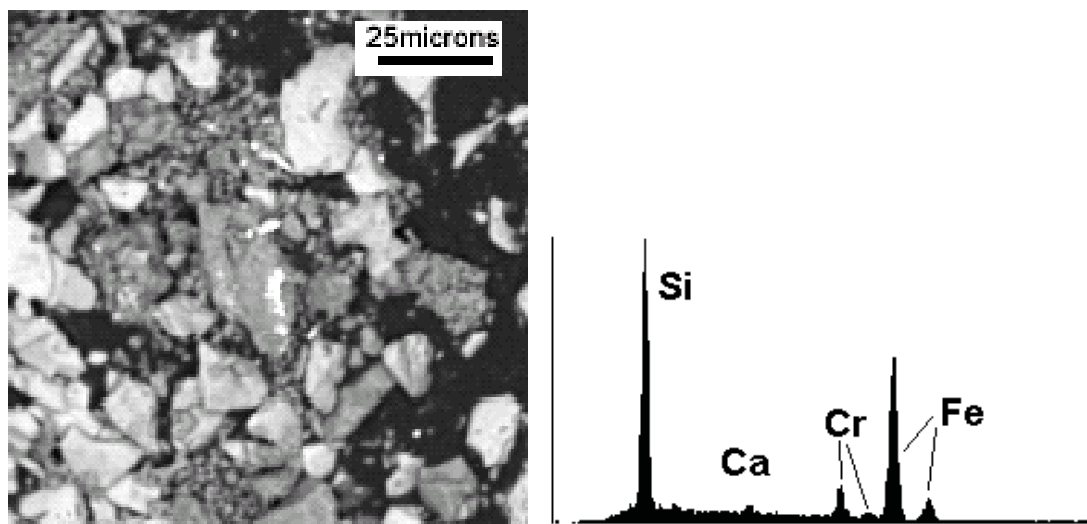
Plate 4.6. Backscatter electron images of HH PG showing quartz (dark grey), gypsum (mid-grey) and Cr-Fe grains (white – centre of picture) with energy dispersive spectra for the latter.

Plate 4.7. SEM image of HH PG from Ardaman (2000). Field of view 15 microns.

4.5   Non-PG Phases

Initial SEM analyses of the crystalline PG indicated that some metal phases were present within the samples, including an iron-chromium compound that is, possibly, the chromite that occurs in the ore (see Sections 4.2.2 and 4.3.2, Plate 4.2 above). As a result of this further sampling was undertaken of the older DH on Cells 1 and 2, newly deposited DH on Cell 4 and HH from the overland conveyor belt (Appendix 3, Appendix 9) to specifically search for other phases contained within the PG.

All the samples were very similar in their non-PG phases. As expected, the primary non-PG mineral was silica (SiO_2) in the form of quartz. The analytical results show that SiO_2 is quite variable, with XRF showing 21.1% in the HH sample (filter cake sampled from the end of the conveyor), 35.6% for the DH sampled directly from the stack (this

is an average of four samples taken at different times and places on the stack with individual results ranging from 14.1% to 61.3%) and 22.3% in the solid component of the slurry (the average of 24 individual samples taken over 12 months with a range of 13.6% to 30.0%). XRD results are even more variable, with the quantitative mineralogy reporting 32% for the HH sample, 22.9% for the DH (range from 16.3% to 29.0%) and 17.8% for the slurry solids (range 2% to 25%).

The SiO_2 content of the ore is known from drilling programs and observations in the pit during mining to be very variable within and between units and parcels (*e.g.* Galah ore tends to be higher in chert than Brolga ore and, despite all of them being high grade phosphate, units 6, 8 and 10 contain significantly more chert than units 2 and 4) so some of this variability can be put down to the ore that was fed to produce any given amount of PG. The sample containing the most SiO_2 (dry stack DH with 61.3% in the XRF results) is most likely due to segregation of coarser grains into the perimeter dyke, as the sample was taken from the outer wall of the stack and SEM examination seems to show that the quartz particles can be much larger than the PG crystals. However, the inconsistency of the XRD results against the XRF results from the same samples suggests that the XRD may be mis-interpreting the results. In the case of the HH sample, it may be possible that the XRD is interpreting soluble silicates, such as the liquid alkali fluorosilicates that cause scaling, as quartz. In the other two samples the XRD is significantly under-representing the amount of quartz present, suggesting that the quantitative mineralogy results can be used, at best, as a guideline only to the mineralogical make-up of the material.

A calcium-phosphate phase was reasonably common within the silica grains (Plate 4.8), as were metal-bearing phases that were predominantly iron occasionally combined with manganese (Plate 4.9). No iron-chromium compounds were found in this series of samples. A single sample contained one grain of barium sulphate (barite - Plate 4.10) which has been identified as occurring within the ore in the Unit 10/Lower Siltstone Member gradational zone (Hough *pers. comm.*. 2003b). An element distribution map of the sample containing the latter is included as Plate 4.11.
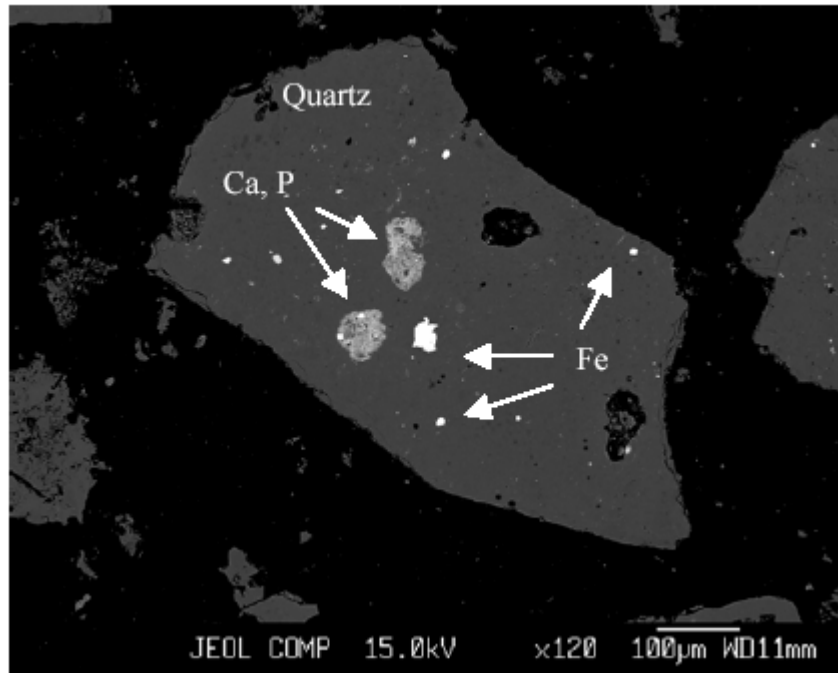
Plate 4.8. Backscatter electron image of quartz grain with inclusions of Ca, P and Fe phases.
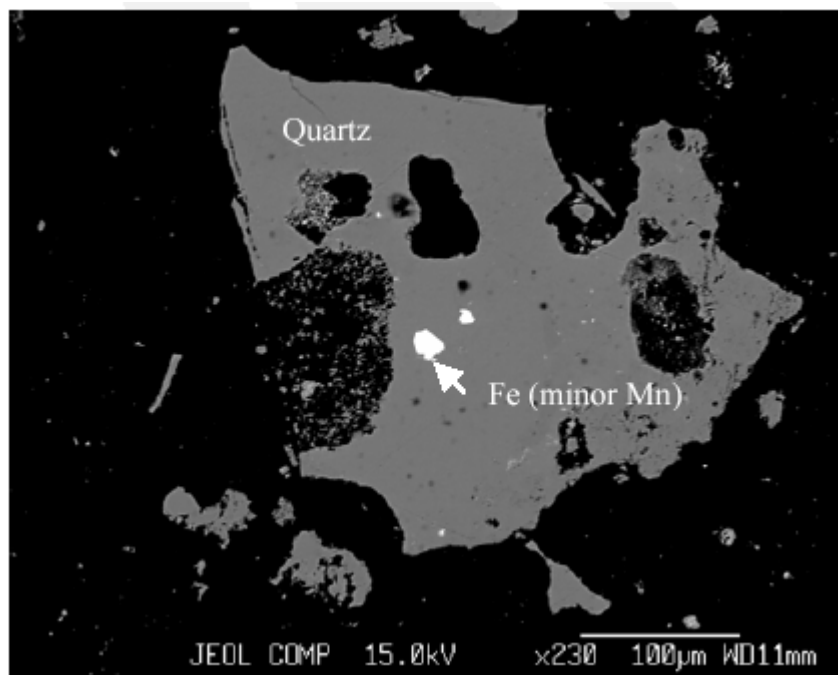

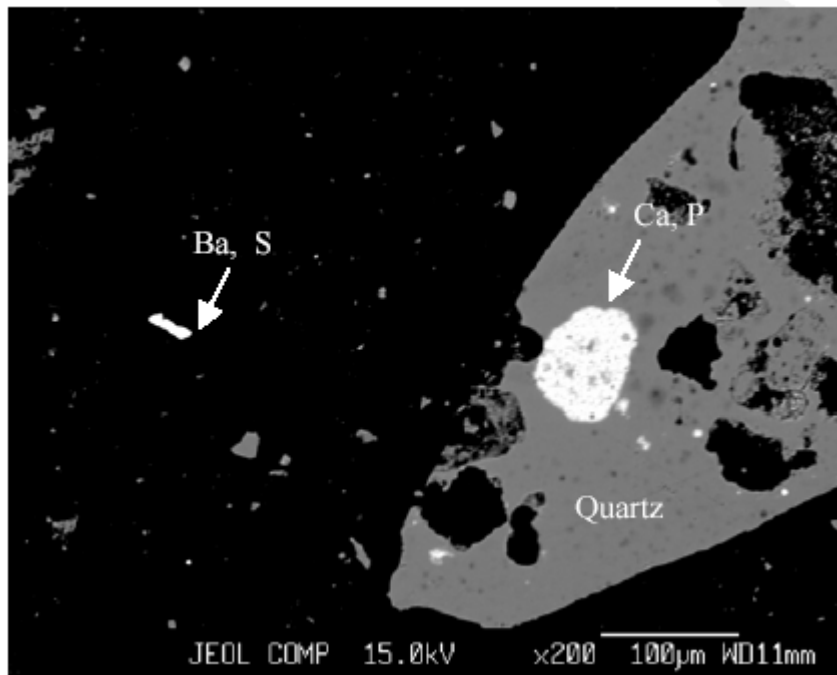**Plate 4.9. Backscatter electron image of quartz grain with inclusions of Fe,Mn phase.**

Plate 4.10. Backscatter electron image of quartz grain with inclusions of Ca, P phase and isolated barium sulphate crystal.
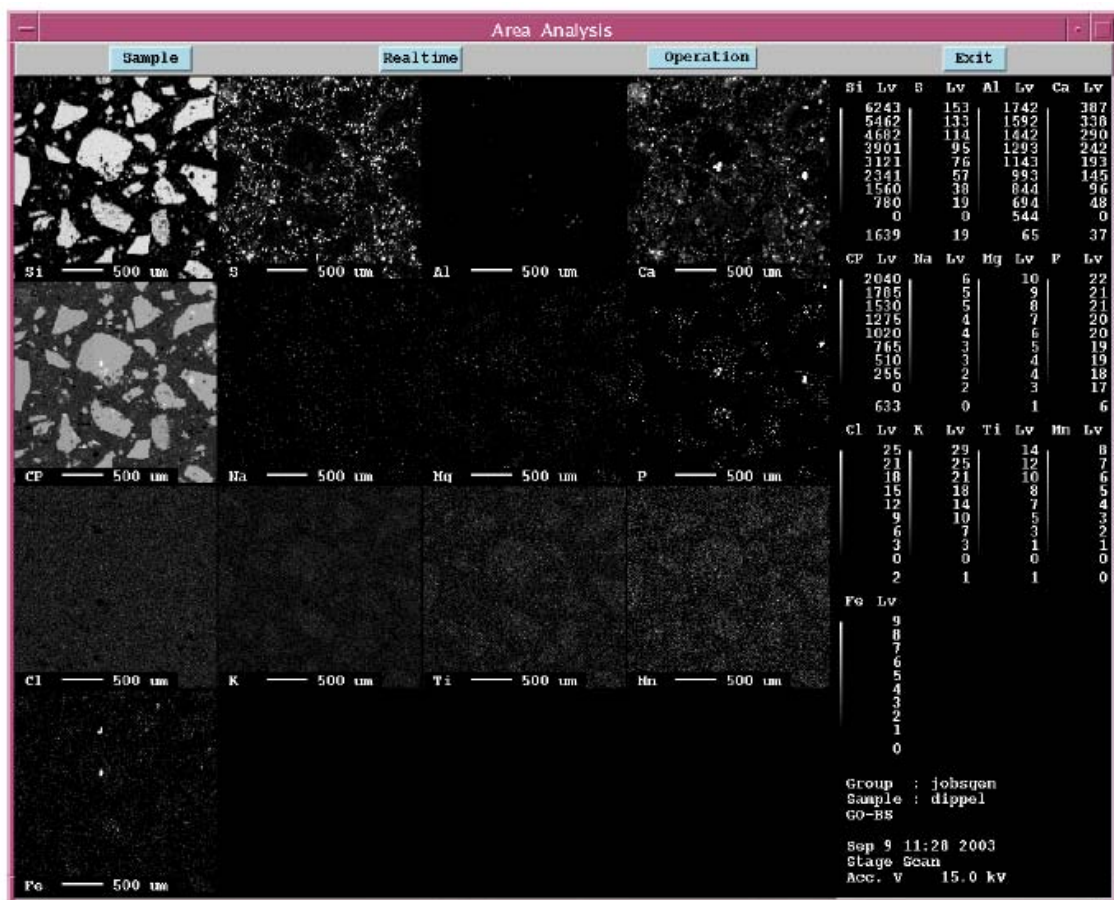

Plate 4.11. Element distribution map of sample GO-BS. Elements displayed separately. CP = backscatter image of sample.

4.6   Dissolution Columns

The PG for each column was analysed for its chemistry and mineralogy both before and after the dissolution process. The analyte was tested separately for chemistry (major and trace elements), nutrients (phosphate), pH and conductivity.   A blank sample consisting of the water used to perform the leaching was included in each sample run. HEMI (or HH) is the hemihydrate leach column; GYP_N (GN) is that containing newly-deposited DH PG fresh from the re-slurry tank, thus containing higher amounts of liquor; and GYP_O (GO) is DH PG deposited 3-6 months previously on the stack and drained of most of its liquor. All results are contained within Appendix 7.

4.6.1   PRE-DISSOLUTION PG ANALYSES

	wt %		
	HEMI	**GYP_N**	**GYP_O**
SiO$_2$	21.1	14.1	37.8
TiO$_2$	0.03	0.02	0.03
Al$_2$O$_3$	0.37	0.31	0.50
Fe$_2$O$_3$T	0.08	0.03	0.12
MnO	0.02	0.01	0.03
MgO	0.03	0.04	0.06
CaO	20.04	20.25	14.86
Na$_2$O	0.11	0.08	0.11
K$_2$O	0.08	0.06	0.09
P$_2$O$_5$	2.16	2.32	3.78
SO$_3$	40.17	41.59	29.52
LOI	15.2	20.6	12.3
SUM	100.0	100.0	100.0

Table 4.15.   Pre-dissolution major element analyses (XRF)

Major element analyses show that CaO, SO$_3$, SiO$_2$ and P$_2$O$_5$ are the dominant phases in the crystalline gypsum phases. F was not detected in any of the samples. The major difference of note between the samples is that the aged PG has a relatively lower proportion of CaO and SO$_3$ and a relatively higher SiO$_2$, suggesting either that this sample contained more SiO$_2$ due to its parent ore, or a more remote possibility that some leaching had already taken place within the material as it had been exposed to intermittent rainfall during its deposition in the wet season of 2001/2002.

	ppm		
	HEMI	GYP_N	GYP_O
As	3	12	7
Ba	329	250	251
Co	7	10	11
Cr	56	43	64
Cu	21	25	25
Mn	139	284	492
Nb	bd	bd	bd
Ni	4	11	9
Pb	12	10	9
Sc	9	4	6
Sr	348	354	267
Ti	193	195	166
V	18	22	34
Y	152	94	112
Zn	27	48	45
Zr	3	1	5

Table 4.16.   Pre-dissolution minor element analyses (XRF)

Minor element analyses were, as expected, dominated by Ba, Mn, Sr, Ti and Y. The aged DH PG sample was relatively enriched in Mn and depleted in Sr compared to the other samples.

Mineralogy (%)	HEMI (%)	GYP_N (%)	GYP_O (%)
Quartz (SiO_2)	32.0	16.30	27.50
*Gypsum ($CaSO_4.2H_2O+*.0.5H_2O$)	43.0	82.90	56.20
Anhydrite ($CaSO_4$)	1.0	1.00	7.00
Bassanite ($CaSO_4.0.5H_2O$)	25.0	0.0	8.00
Expanding clays	0.0	0.0	1.00

Table 4.17.   Pre-dissolution quantified mineralogy.   *The specification of $CaSO_4.2H_2O+*.0.5H_2O$ is the total of standard dihydrate gypsum plus dihydrate with additional partial or complete molecules of water attached to it.

Quartz was variable between the three samples, as were the individual percentages of gypsum species. Bassanite was higher and DH gypsum was lower in the HH sample, as expected, compared to levels in the DH columns.

4.6.2   POST-DISSOLUTION PG ANALYSES

	wt %		
	HEMI	**GYP_N**	**GYP_O**
SiO$_2$	25.3	13.8	43.9
TiO$_2$	0.04	0.04	0.05
Al$_2$O$_3$	0.43	0.30	0.51
Fe$_2$O$_3$T	0.09	0.02	0.14
MnO	0.01	0.00	0.01
MgO	0.07	0.05	0.07
CaO	23.7	27.0	17.2
Na$_2$O	0.00	0.00	0.00
K$_2$O	0.05	0.03	0.07
P$_2$O$_5$	0.75	0.43	0.55
SO$_3$	27.9	33.4	20.2
F	0.3	0.2	0.2
LOI	22.2	24.9	17.1
SUM	100.6	100.0	99.9

Table 4.18.   Post-dissolution major element analyses (XRF).

Post-dissolution major element analyses show only minor relative changes in SiO$_2$. However, significant falls in SO$_3$ and P$_2$O$_5$ and increases in CaO were recorded compared to pre-dissolution figures.   The loss of P$_2$O$_5$ would most likely be through loss of H$_3$PO$_4$ in the pore spaces of PG.   The drop in SO$_3$ may be partly due to the loss of the relict H$_2$SO$_4$ that is a significant proportion (along with HF and H$_3$PO$_4$) of the acid process water that is used to re-slurry the HH filter cake (Duckworth 1997) and would thus also be held within the pore spaces of the PG, rather than solely through loss of colloidal gypsum and dissolution of the solid phase.   F was found to be present at very low levels in the post-dissolution material.   The increase in CaO recorded post-dissolution is a most unlikely result and is probably due to problems within the analytical process, such as incorrect calibration or contamination.   Other elements also shows minor depletion post-dissolution.

	ppm		
	HEMI	**GYP_N**	**GYP_O**
As	1	bd	5
Ba	295	250	366
Co	5	4	5
Cr	52	29	73
Cu	14	13	12
Mn	6	bd	30
Nb	bd	bd	1
Ni	1	bd	1
Pb	18	21	6
Sc	8	5	5
Sr	332	367	207
Ti	205	207	234
V	8	10	16
Y	112	88	61
Zn	15	14	16
Zr	2	1	9

Table 4.19.   Post-dissolution minor element analyses (XRF).

Minor element trends in the post-dissolution analyses shows variable depletion of most element, most notably in Mn and Ni in all columns. Enrichment in Ti was found in all samples, of Pb in two samples (Hemi and Gyp_N), in Sc and Sr for Gyp_N alone and in Ba and Cr in Gyp_O. Possible reasons for this enrichment are discussed in Chapter 5.7.

Mineralogy (%)	HEMI (%)	GYP_N (%)	GYP_O (%)
Quartz (SiO_2)	31.50	13.70	32.40
*Gypsum ($CaSO_4.2H_2O+*.0.5H_2O$)	65.60	80.20	61.90
Anhydrite ($CaSO_4$)	6.00	0.00	0.00
Bassanite ($CaSO_4.0.5H_2O$)	2.30	6.10	3.70
Expanding clays	0	0	2.00

Table 4.20.   Post-dissolution quantified mineralogy.   *The specification of $CaSO_4.2H_2O+*.0.5H_2O$ is the total of standard dihydrate gypsum plus dihydrate with additional partial or complete molecules of water attached to it.

A comparison of pre- and post-leach solid mineralogy reveals notable trends. Graphs for quartz (SiO_2), bassanite ($CaSO_4.0.5H_2O$), dihydrate gypsum ($CaSO_4.2H_2O$) and anhydrite gypsum ($CaSO_4$) are shown in Figures 4.15 to 4.18 below.
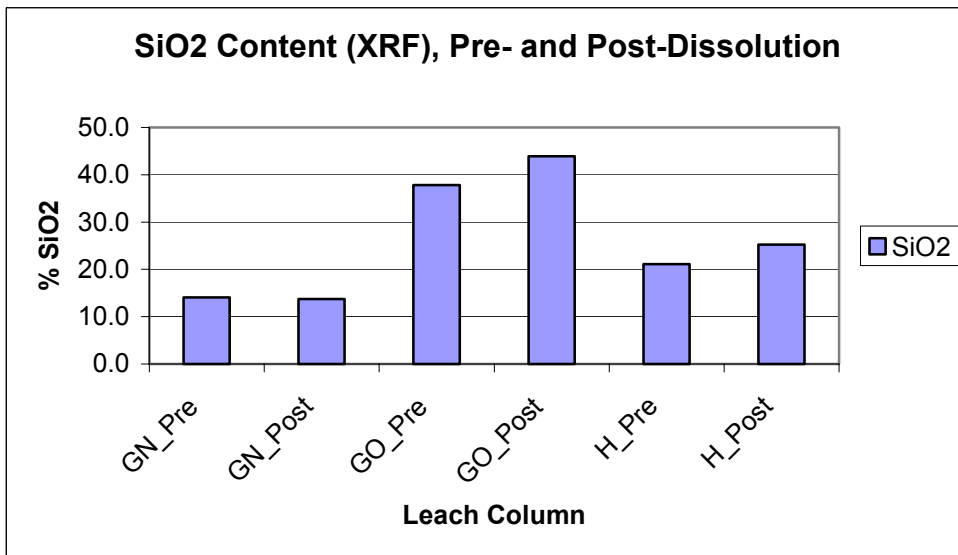
Figure 4.15. Pre- and post-dissolution SiO$_2$ content (XRF), all columns.

SiO$_2$ showed a minor fall after the dissolution process in the newly-deposited PG sample. It recorded a rise post-dissolution in both the aged DH and the HH columns. Possible causes of this variability are also discussed in Chapter 5.7.
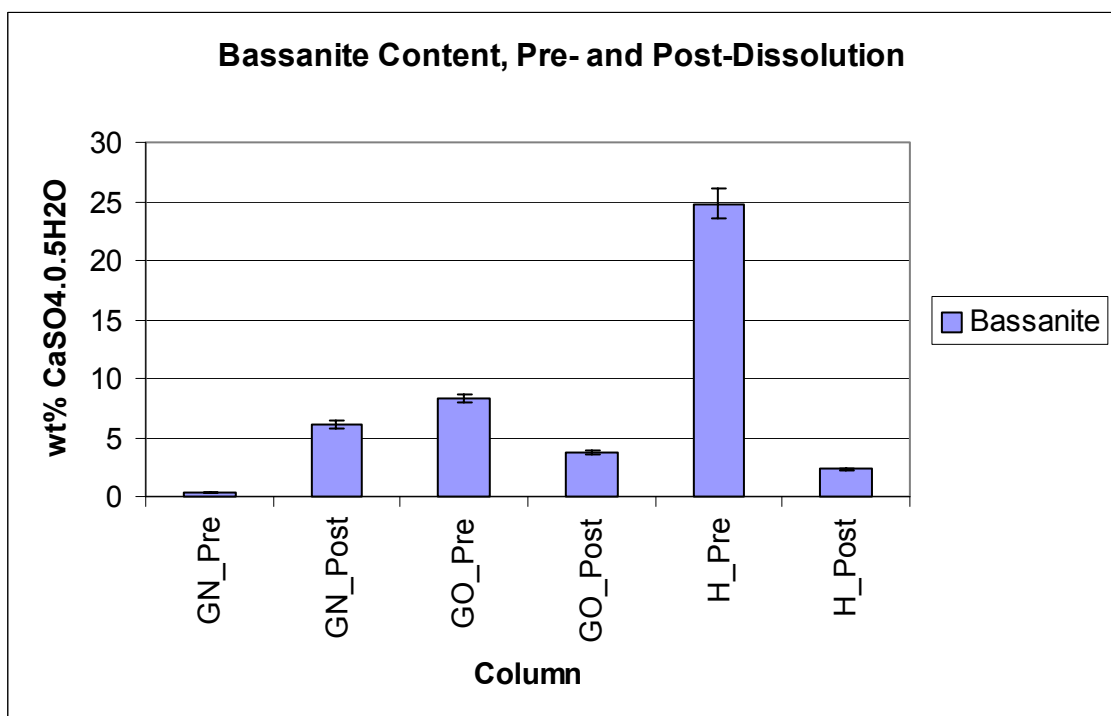
Figure 4.16. Pre- and post-dissolution bassanite (CaSO$_4$.0.5H$_2$O) content (XRD), all columns.

As expected, there was a fall in the bassanite ($CaSO_4.0.5H_2O$) content during the dissolution process. However, this occurred only in the HH and aged DH columns, while the fresh DH showed a massive increase. Although there may possibly be a very small increase in this material post-dissolution due to incomplete conversion processes, particularly in the hydration of the anhydrite recorded pre-dissolution in the same sample (Figure 4.18), where some anhydrite ($CaSO_4$) may have been only semi-hydrated ($CaSO_4.0.5H_2O$), instead of fully hydrated ($CaSO_4.2H_2O$) when sampled, a 20-fold increase is extremely unlikely. Thus, this result is almost certainly wrong and probably represents mis-identification of the gypsum species by the XRD process.
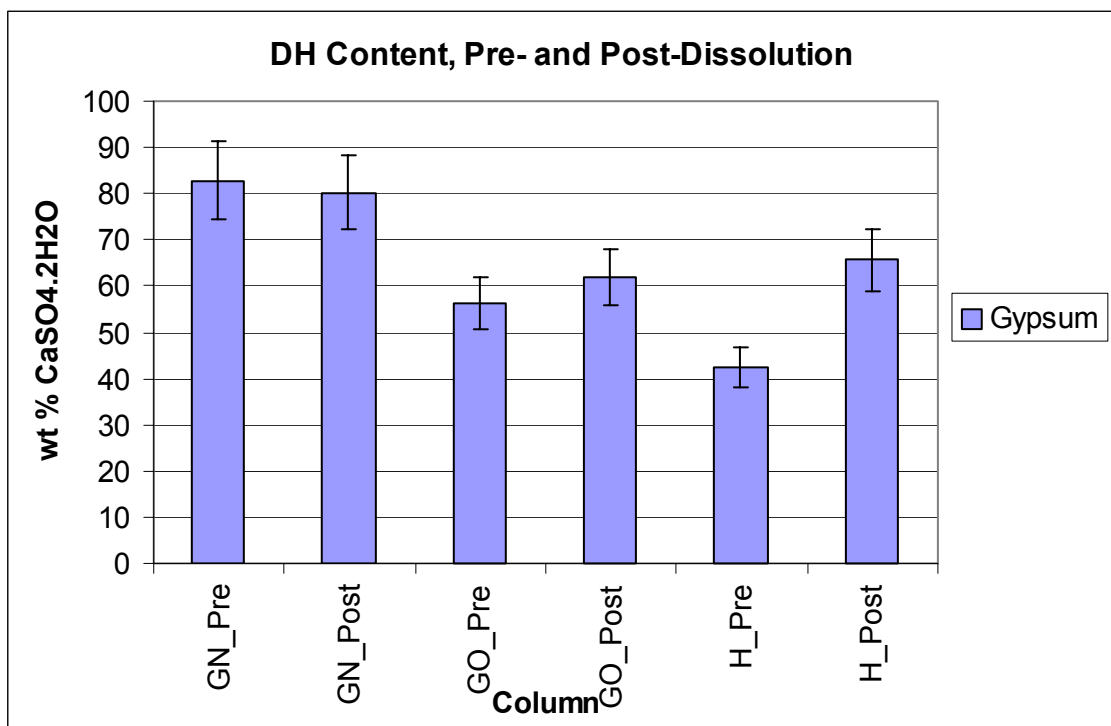
Figure 4.17. Pre- and post-dissolution DH ($CaSO_4.2H_2O$) content (XRD), all columns.

Dissolution caused the amount of DH ($CaSO_4.2H_2O$) to fall very slightly in the newly-deposited material. This may reflect the post-dissolution increase in HH in this column (Figure 4.16) possibly due to either incomplete conversion processes, unaccounted-for differences between the mass sample analysed before the dissolution and the sub-sample in the column analysed post-dissolution or (most likely) misidentification of HH for DH. In the aged DH the DH content rose slightly whilst the HH column showed a notable increase in DH, reflecting the dramatic fall in HH content in that column recorded over the dissolution period (Figure 4.16).
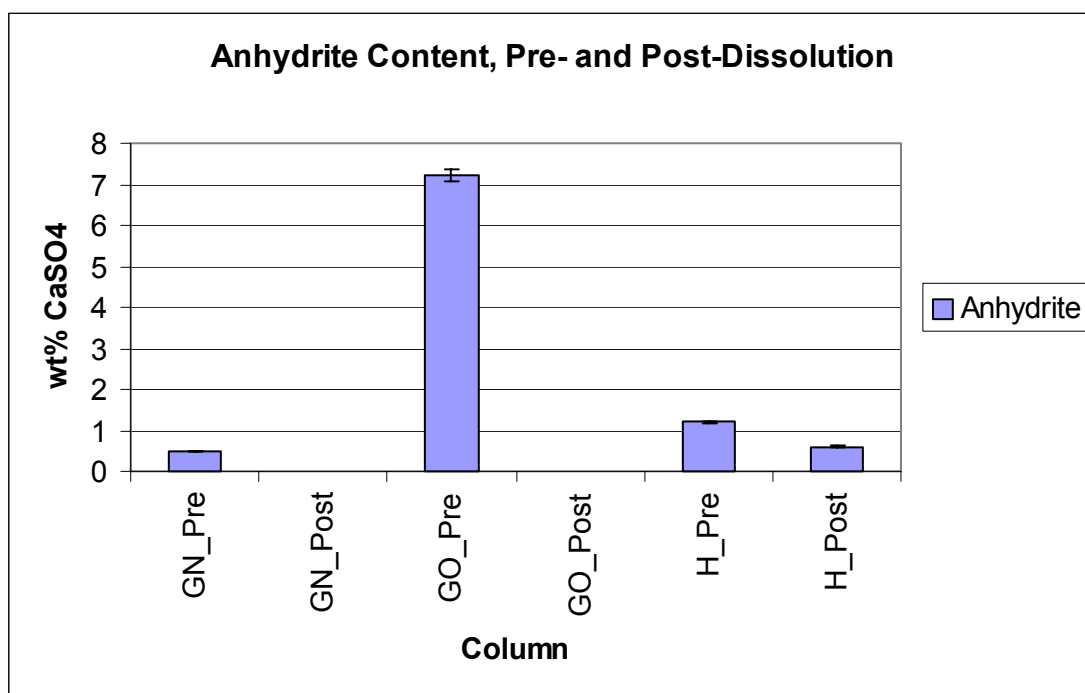
Figure 4.18. **Pre- and post-dissolution anhydrite (CaSO₄) content (XRD), all columns.**

Anhydrite (CaSO₄) content was removed completely during the dissolution process in both DH columns and considerably reduced in the HH column. This probably represents the hydration or rehydration of the anhydrite either partially to bassanite or completely to dihydrate gypsum. Relative changes pre- and post-dissolution for mineralogy are summarised in Table 4.21 below.

% change	Gypsum	Anhydrite	Bassanite	Quartz
GYP_N	-3.3	-100	+20x*	-15.9
GYP_O	+10.1	-100	-53.7	+17.8
HEMI	+52.3	-50	-90.8	-1.6

Table 4.21. **Quantified mineralogy relative changes, from the pre- to the post-dissolution stage, for new and old DH and HH columns. *This result is almost certainly wrong, probably due to mis-identification of the gypsum species.**

Pre- and post-dissolution comparisons between major and trace element contents in the column material are presented in Figures 4.19 to 4.20b.
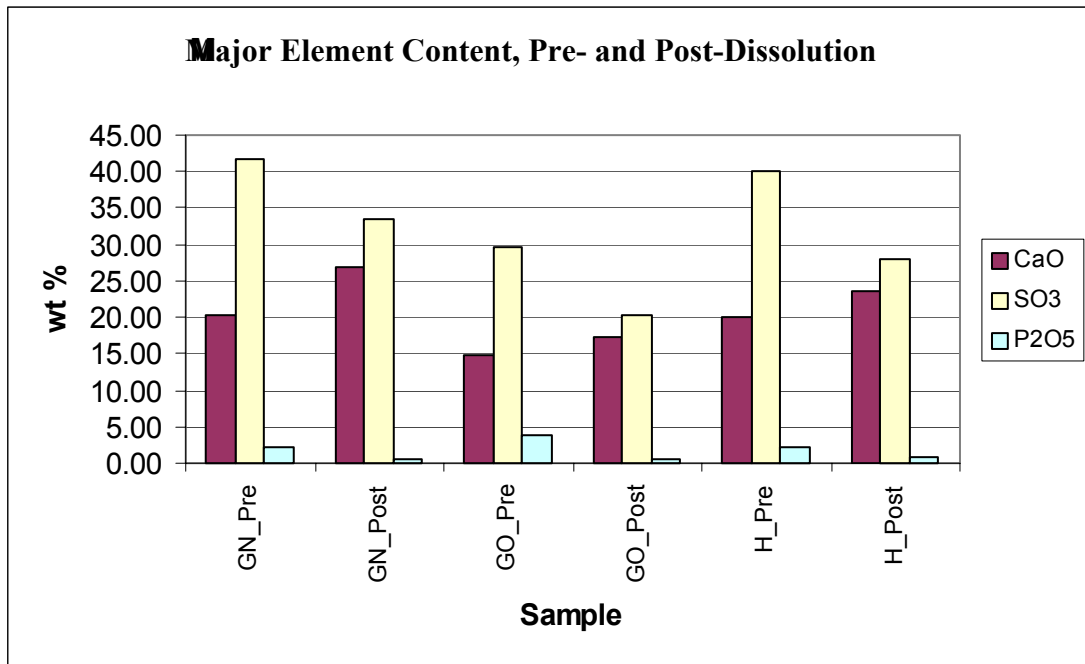
Figure 4.19a. **Primary major element content (XRF), pre- and post-dissolution, all columns.**

The dominant major elements in the columns are shown in Figure 4.19a. All columns showed a drop in SO_3 and P_2O_5 levels and an increase in SiO_2 and CaO. The drop in the former would reflect the higher solubilities of calcium sulphate and calcium phosphate in water. The results showing a post-dissolution increase in CaO are of some concern, as an increase in CaO combined with a loss of SO_3 is extremely unlikely. This particular set of results would appear to be flawed and may be the result of contamination of the samples or incorrect calibration of the machine. Relative changes are summarised in Table 4.22 below.

% change	P_2O_5	SO_3	CaO	SiO_2
GYP_N	-81.5	-19.7	+33.3	-2.2
GYP_O	-85.3	-31.4	+15.5	+16.1
HEMI	-65.3	-30.7	+18.3	+19.5

Table 4.22. **Major element changes, from the pre- to the post-dissolution stage, for new and old DH and HH columns.**
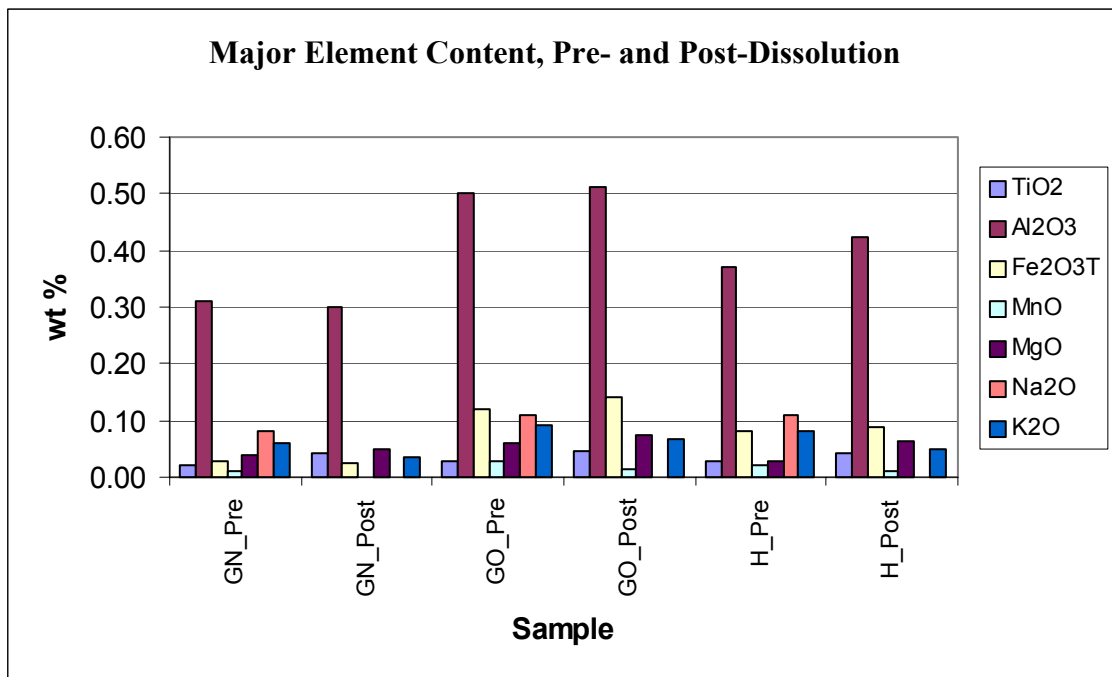
Figure 4.19b. **Secondary major element content (XRF), pre- and post-dissolution, all columns.**

Pre- and post-dissolution comparisons of secondary major elements in the PG are shown in Figure 4.19b. Post-dissolution falls were recorded in MnO, Na_2O and K_2O, a minor rise in TiO_2 and the remaining elements were variable and showed little real change in their concentration levels. Na_2O levels, particularly in the GN sample, were very close to the lower limit of detection (0.04 wt%) and may be unreliable.
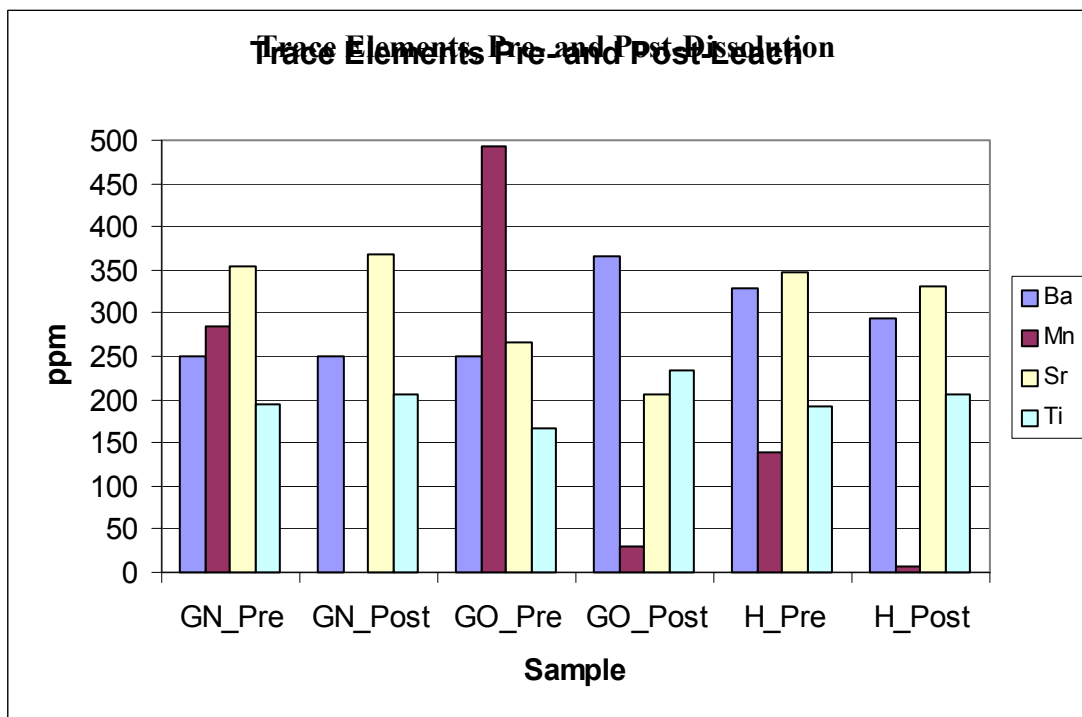
Figure 4.20a. Primary trace element content (XRF), pre- and post-dissolution, all columns.

Primary trace element trends are displayed in Figure 4.20a. Mn shows a dramatic post-dissolution drop and Ti has a slight increase in all three columns. Ba and Sr are variable. Secondary trace elements illustrated in Figure 4.20b show similar variability in Cr, Pb and Sc but all other elements display a fall in levels post-dissolution. Nickel shows the greatest consistent losses post-dissolution, with a drop of between 75% and 100%, with Zn (44%-71%), Co (28% to 60%) and As (29% to 100%) also displaying large falls.
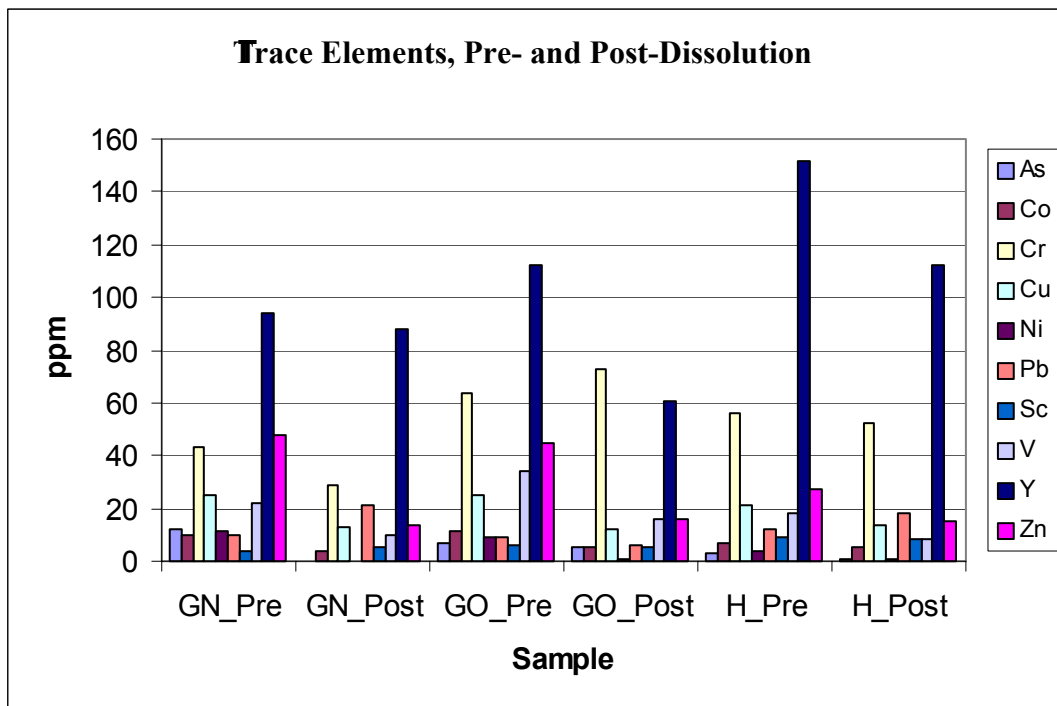
Figure 4.20b. Secondary trace element content (XRF), pre- and post-dissolution, all columns.

The majority of the losses in all elements occurred during the first flushing event (Figures 4.23-4.29 inclusive). Such analyses indicate that column leachates should be enriched in sulphate and metals such as manganese, nickel and zinc (see Figures 4.27-4.29 inclusive).

4.6.3   ANALYTE RESULTS

Four flushing events were carried out on all columns. The PG was allowed to dry out between events in order to simulate the effect of the sporadic large rain and flood events that are typical of the wet season at Phosphate Hill. It should be noted that Flush 5 was only carried out on sample GYP_O. This was after it was discovered that there was a shortfall in the water input into that column after the completion of the first four flushes. The extra flush was carried out immediately after Flush 4, with no drying period between the two, and so is more a continuation of Flush 4 rather than a completely separate event.
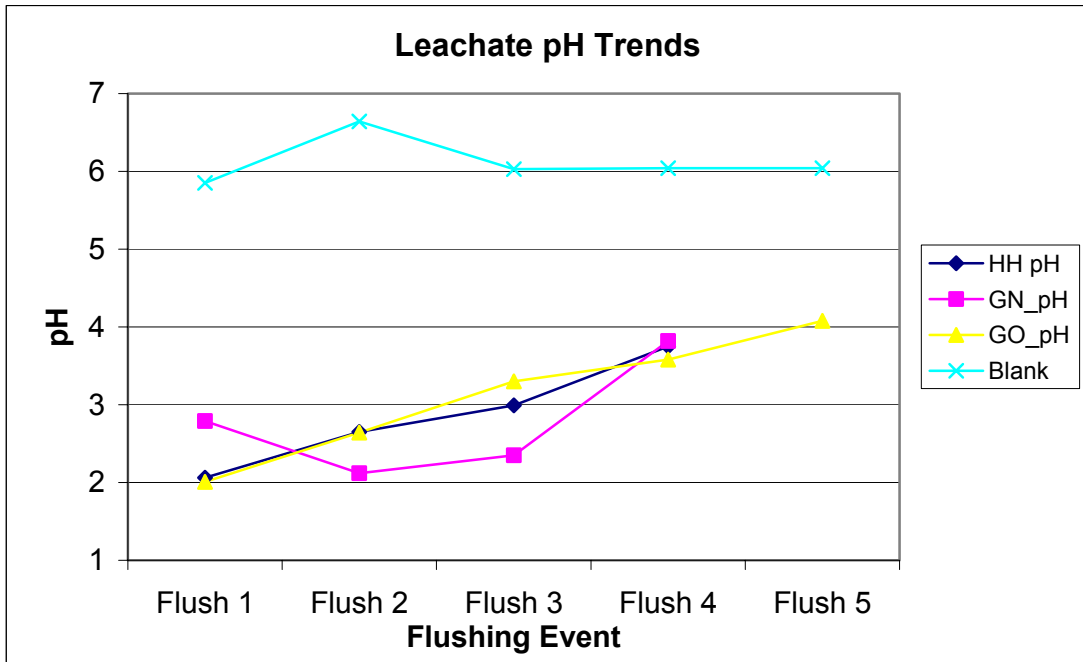
Figure 4.21. pH trends in leachate, all columns.

Figure 4.21 displays the pH trends for all leach columns over the course of the flushing exercise. The overall trend for all leachate is an increase in pH towards neutral with ongoing flushing.
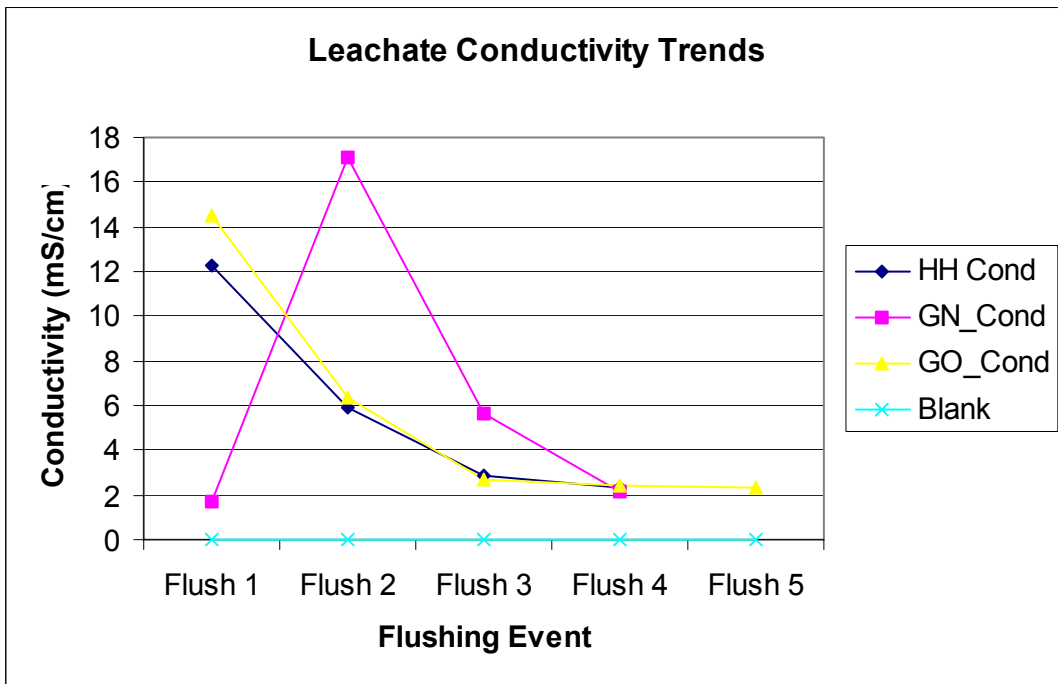
Figure 4.22. Conductivity trends in leachate, all columns.

Conductivity trends during leaching are shown in Figure 4.22. A decreasing trend is evident in all columns. The first reading for GN appears to be anomalous, as do many of the other initial readings for this sample's leachate (*e.g.* Figures 4.21, 4.22, 4.25)
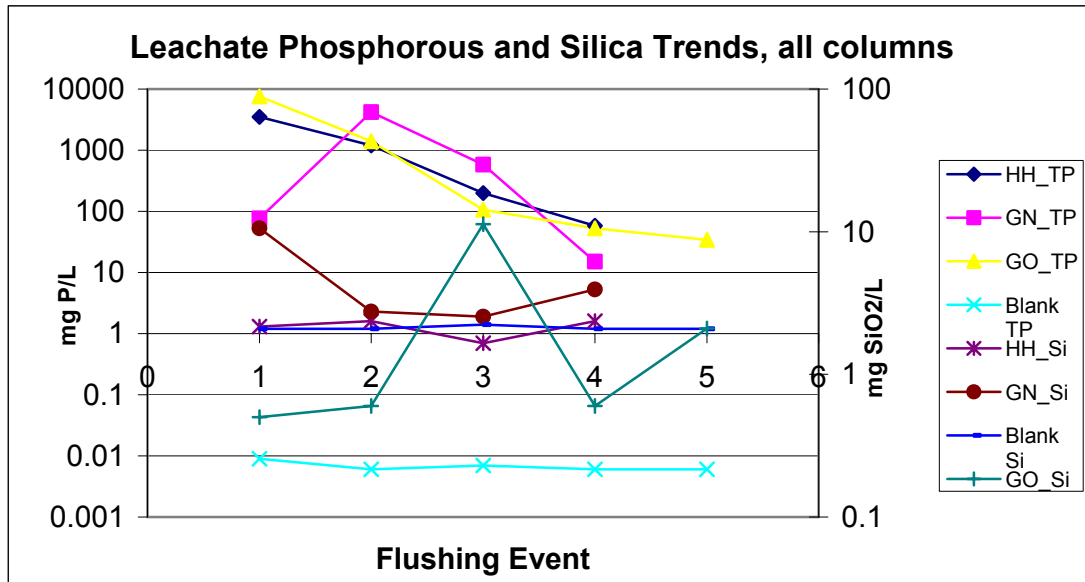
Figure 4.23. **Phosphorous and silica trends in leachate, all columns.**

Phosphorous and silica trends during leaching are shown in Figure 4.23. Total P falls while silica shows a very slight increase. Filterable reactive phosphorous (the soluble portion of Total P that is readily available as an algae and plant nutrient) follows much the same trend as Total P.

Leachate trends for major elements are shown in Figures 4.24 to 4.26. Each figure refers to an individual column.
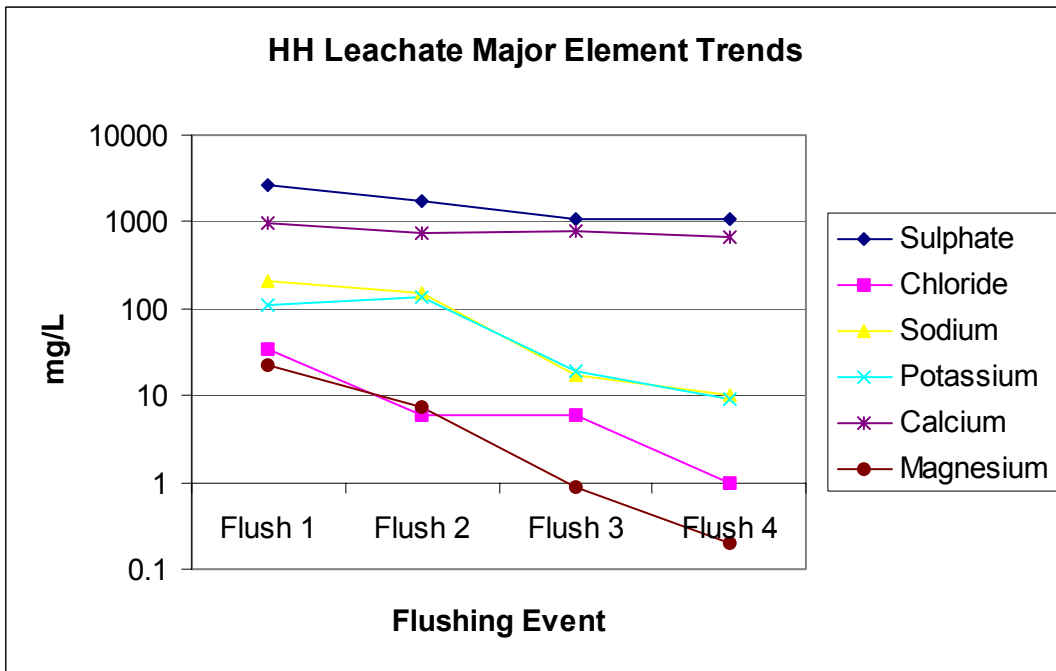
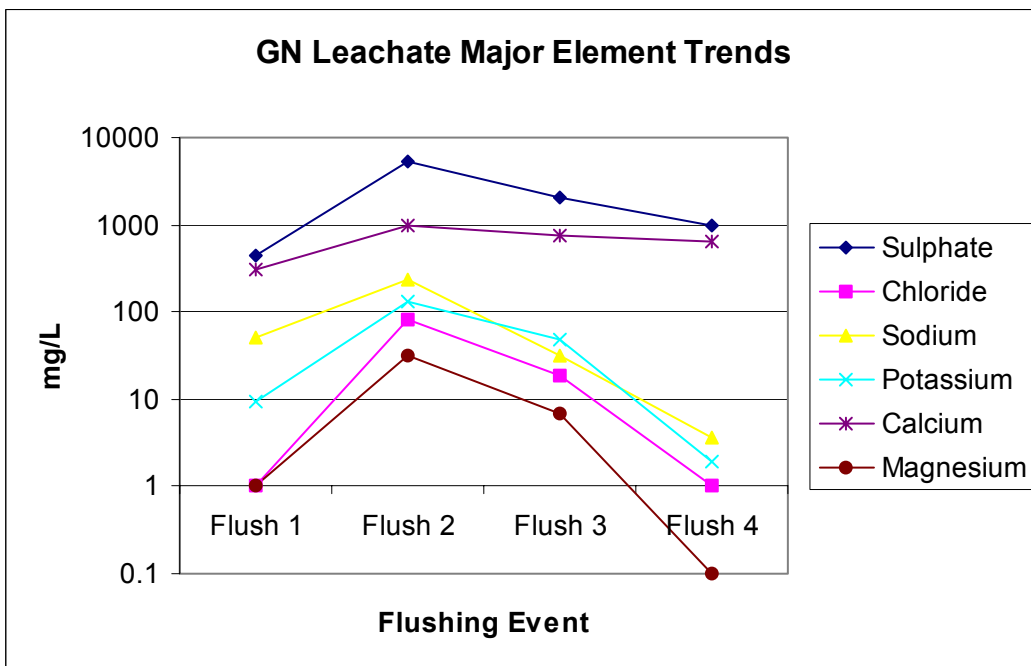**Figure 4.24**. Major element trends in leachate, hemihydrate column.

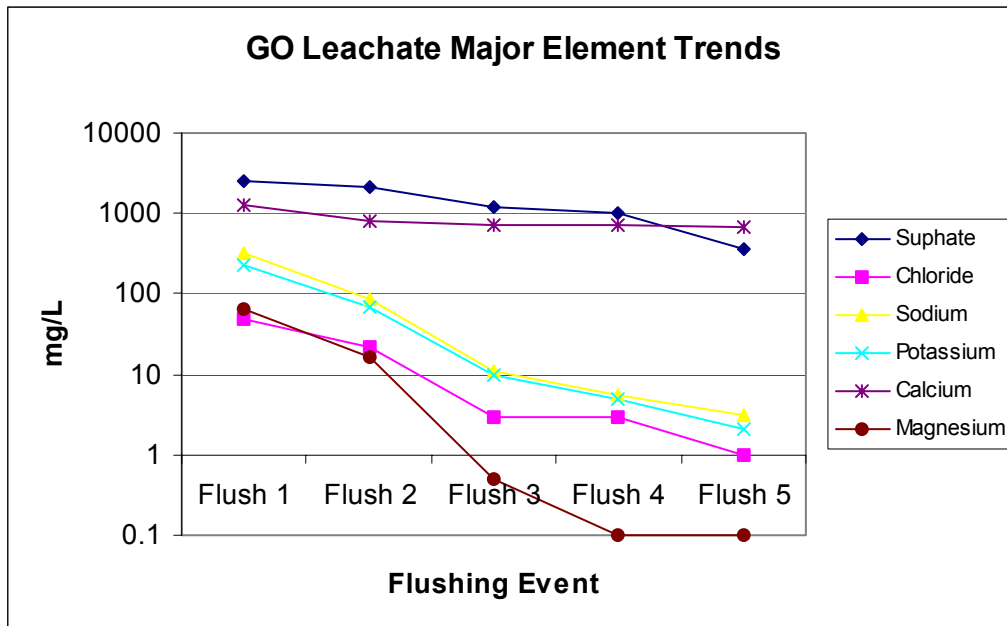**Figure 4.25**. Major element trends in leachate, freshly-deposited DH column.

Figure 4.26. Major element trends in leachate, aged DH column.

All major elements show distinctly decreasing trends over the course of the leaching. The greatest amount of leaching appears to occur in the first two to three flushing events. There again appears to be an anomaly with the initial readings on column GN, which is repeated in the trace element results for the same column (Figure 4.28). This recurring pattern suggests that the newly-deposited PG behaves in a quite different manner to the other types tested, not releasing the majority of its leachable ions until the second flushing event. Sulphate and calcium levels follow similar trends in the analyte, which tends to confirm that the post-dissolution increases recorded in the XRF results are an error.
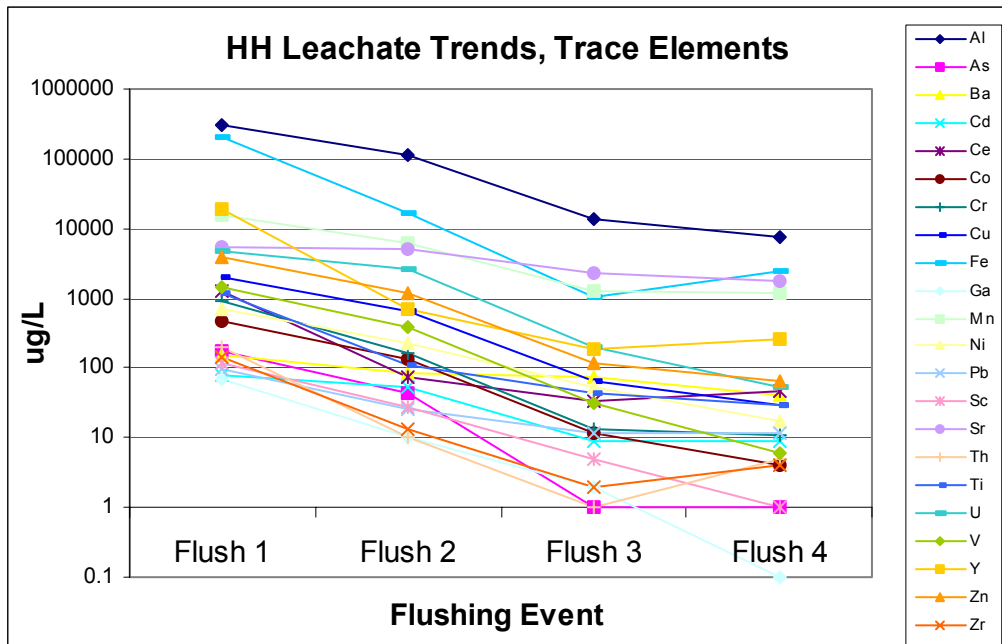
Figure 4.27. **Trace element trends in leachate, HH column.**

All trace elements show a consistent falling trend for the first three flushing events, most then flattening off. Levels of Fe, Y, Th and Zr, however, rose slightly in the final flush.
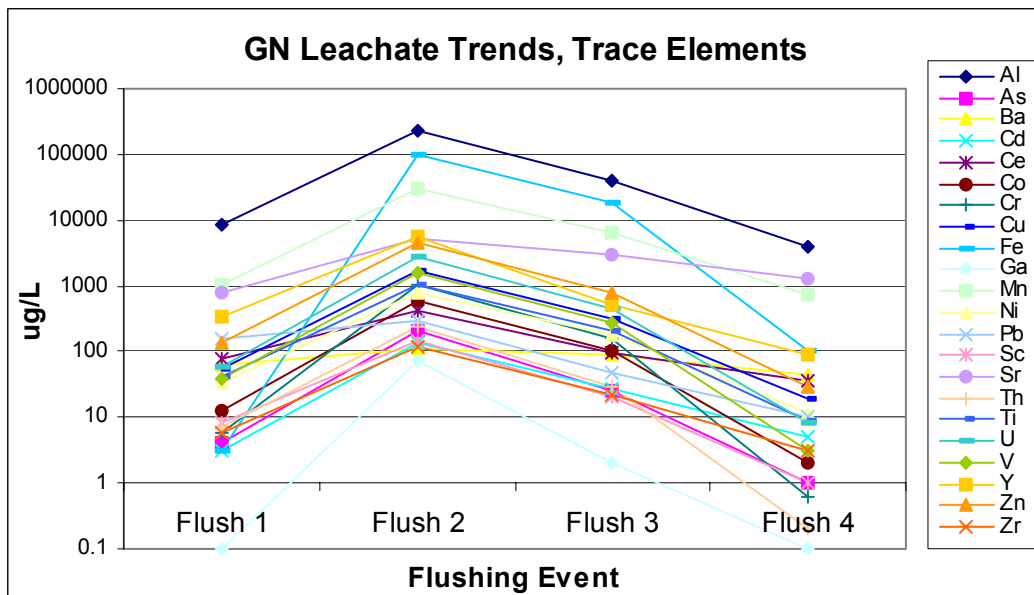

Figure 4.28. Trace element trends in leachate, freshly deposited DH column.

The freshly deposited DH again showed an increase in levels on the second flushing event, in contrast to the other two columns, but thereafter all elements fell consistently. As this peak seems to be a consistent pattern in this sample it strongly suggests that the material behaves differently to the others, for reasons not currently identified.
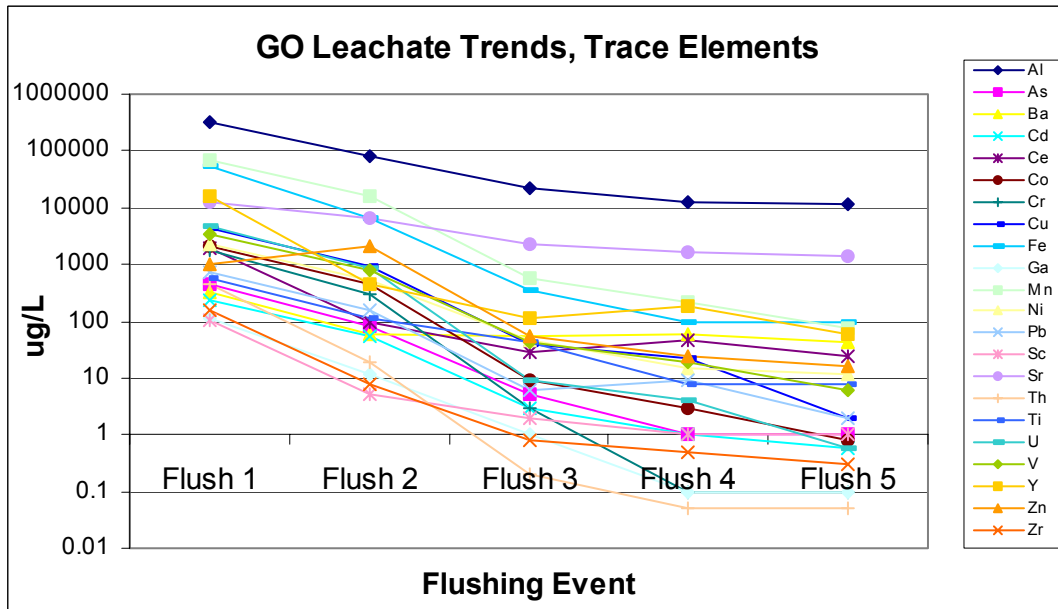

Figure 4.29. **Trace element trends in leachate, aged DH column.**

The aged DH in the third column was the most consistent of the three in its dissolution behaviour. All elements fell sharply in the first three flushing events with trends then flattening off.

The trends shown by all columns suggest that, given time and a sufficient volume of liquid passing through the PG, the PG will eventually be stripped of its mobile components. This will result in leachate that, over the long-term, should begin to approach neutral levels.

4.6.4   PHYSICAL RESPONSE OF PG TO ADDITION OF WATER

In addition to chemical analysis of the PG both pre- and post-dissolution, observations were made on the physical state of the material loaded into the columns after each flushing event. The amount of water going into the columns in Table 4.23 below is not

consistent due to the requirements to obtain a minimum of 100ml of leachate per episode and the reaction of each type of PG to the addition of water.

	WATER IN	LEACHATE OUT	WATER RETAINED (ml)	WATER RETAINED (%)
HH Flush 1	180	108	72	40
Flush 2	125	102	23	18.4
Flush 3	175	140	35	20
Flush 4	160	107	53	33.1
HH TOTAL	**640**	**457**	**183**	**28.6**
NEW DH Flush 1	140	121	19	13.6
Flush 2	125	105	20	16
Flush 3	305	204	101	33.1
Flush 4	175	87	88	50.3
"FRESH" DH TOTAL	**745**	**517**	**228**	**30.6**
OLD DH Flush 1	140	110	30	21.4
Flush 2	125	113	12	9.6
Flush 3	125	104	21	16.8
Flush 4	150	110	40	26.7
Flush 5	130	121	9	6.9
"AGED" DH TOTAL	**670**	**558**	**112**	**16.7**

Table 4.23.   Water retention rates of PG columns

The following sections 4.5.4.1-4.5.4.3 are summaries of the reaction of the dissolution column contents to the addition of water. It should be noted that there was a 14 day delay between loading of PG into the columns and the first water input, due to the need for further clarification on some technical details of the dissolution process and the WMCF roster requirements.

4.6.4.1 Hemihydrate PG

Hemihydrate (HH) PG ($CaSO_4.0.5H_2O$) is the direct result of the acidulation process within the phosphoric acid plant reactors. The slurry is piped from the reactors to the filter floor where the PG is filtered from the acid and transported *via* overland conveyor to the re-slurry tank at the southern end of the gypsum stacking area.

4.6.4.1(i)   Age

The HH sample was obtained from the end of the overland conveyor as the material is deposited into the re-slurry tank (Plate 3.5). It is fresh material derived directly from the acid filter floor of the phosphoric acid plant and as such is approximately 5-10 minutes old.

4.6.4.1(ii)   Particle Size

The material was a just-moist powder. WMCF assays reveal that the HH filter cake was measuring approximately 23.7% moisture on the sampling date, 25.4.02. The material was immediately sealed into its plastic sample container and should not have lost moisture during the transporting period before it was loaded into the columns on 29.4.02. During the delay period the column was covered but there may have been some water loss. However, it still appeared to be damp on the occasion of the first water input. Particles were extremely fine, <<1mm in diameter (25-50 microns average from SEM data).

4.6.4.1(iii)   Dissolution Behaviour

Throughout the dissolution process water consistently passed straight through this material with no impediment to the flow.

4.6.4.1(iv)   Particle Growth

After the first water addition the particles were noted to have aggregated into much larger, granular clumps, up to 2mm diameter. This tendency to aggregate continued with further addition of water and by the end of the experiment some of the clumps were up to 3mm in diameter.

4.6.4.1(v)   Water Retention

28.6% of the total water passed through the column was retained by the PG (Table 4.21). The majority of water retention occurred during the first flushing event, with

40% of the input water (72ml out of 180ml) being retained. The fourth and final flushing event also retained a high volume of the water, at 33% or 53ml out of 160ml.

4.6.4.2 "New" Dihydrate PG

4.6.4.2(i)   Age

The "new" DH consisted of freshly deposited material pulled out of the rim ditch by the excavators. This usually occurs 3-5 days after conversion from HH to DH in the re-slurry tank and decanting into the stack as the material is given time to build up in the rim ditch before the discharge spigot is moved and the excavators commence building the next level of the dykes (Figure 2.15).

4.6.4.2(ii)   Particle Size

The DH was a fine to coarse grained, very damp "sand" (aggregates of average 50 micron diameter with individual grains <20 microns in length and some larger quartz particles up to 500 microns in diameter) when sampled. Due to the high fluid content associated with this material (Ardaman 2000 report a moisture content of 41.5% at 40ºC) the sample partly liquefied during transport. Liquefaction is a known hazard associated with freshly deposited PG and can also occur in older material with repeated applications of pressure (such as vehicles moving over the same tracks). This is illustrated in Plate 4.12, which shows a 30 tonne long-arm excavator that has sunk to the base of the cabin due to liquefaction of the perimeter dyke material underneath it.

Plate 4.12   30 tonne excavator sunk into perimeter dyke PG, Cell 1, Phosphate Hill, April 2000. The excavator body sank until it was floating on the base of the cabin and the bucket was also completely submerged in liquefied PG.

4.6.4.2(iii)   Dissolution Behaviour

The material hardened slightly between the loading of column and the first water input. Initial water transport was straight through but times vastly increased on following occasions due to slow drip rate through hardening material, from 60 minutes on the second occasion to up to 3.5 days for each of the remaining inputs.

4.6.4.2(iv)   Particle Growth

After the first water addition the material "set" quite firmly and appeared to continue to compact with additional water inputs. However, the grain sizes remained very fine and there was no apparent tendency to aggregate into clusters as was seen in the HH.

4.6.4.2(v)   Water Retention

30.6% of the total water passed through the column was retained by the DG (Table 4.21). In contrast to the HH, water retention increased with each flushing episode, the first retaining just over 13% (19ml of 140) of the input liquid and the fourth retaining 50.3% (88ml of 175ml). This meant that extra water (above the allocated 640ml, or 2 years' approximate rainfall) had to be input into the last two flushes in order to gain the required minimum 100ml of leachate for sampling.

4.6.4.3 "Aged" Dihydrate PG

4.6.4.3(i)   Age

This material was sampled from 3-5m below current surface of the gypsum stack. Using average surveyed stack growth rates (Appendix 4) the sample DH was estimated to be between four and six months old.

4.6.4.3(ii)   Particle Size

This DH was a dry, fine-coarse grained sandy powder with aggregate grains up to 1mm in diameter. Moisture content appeared to be low as the sampling area had had time to drain most of its fluids.

4.6.4.3(iii)   Dissolution Behaviour

There was little visible difference evident in the material between loading and first water input. However, initial water transport was notably slower than with the other samples (~10 minutes *cf* ~1 minute). Although not as slow as the new PG on the second input of water, after that the pace of water transport was similar to the new PG, requiring up to 3.5 days to pass through the material. However, on the final input of water the movement through the material was much faster, as it was already wet.

4.6.4.3(iv)   Particle Growth

The material consolidated ("set") in a manner similar to that of the new PG after the first input of water and continued to do so for the rest of the experiment, although the grain size remained small. The DH forms a crust on the stack so this consolidation is in character with known behaviour.

4.6.4.3(v)   Water Retention

16.7% of all the water put into the column was retained by the PG. Similar to the HH column, the greatest water retention occurred on the first and the fourth flushing events, with retention of 21.4% (30ml of 140ml) and 26.7% (40ml of 150ml) respectively. A small amount of extra water was needed with this column on the fifth flush in order to gain the required 100ml of leachate for analysis.

4.7   Radionuclides

An initial examination of radionuclide behaviour throughout the site operations was undertaken by Brown *et al.* (2000). Samples were taken from ore bodies, beneficiation plant, phosphoric acid plant, granulation plant and from the PG stack. The samples included primary products (rock filter cake feed, DAP, phosphoric acid, PG) and by-products, including waste waters, scale and slimes.

Uranium was found to follow phosphate through the system and into the fertilizer product while the majority of the radioactive progeny (Ra-226, Po-210 and Pb-210) went to the PG stack. Thorium appeared to split between product and PG while Po-210 could be present in gases in the plant and Ra-226 was suspected of possibly accumulating in plant scale. The results of this study concluded that uranium and its progeny would not be an issue at Phosphate Hill as levels were low compared to sites elsewhere (Table 5.7) and thus worker exposure would be expected to be below the public dose limit of 1 mSv/y. Thus, the radiological impact of the operation was deemed to be virtually nil.

Part of the current study was to look more closely at the radionuclide levels in the PG. Slurry samples were obtained and sent to the same team at the Australian Nuclear Science and Technology Organisation (ANSTO) for analysis. The new analyses show that although the results for the solids were much the same as those measured in the 2000 study, those for the liquid component were consistently higher (Figures 4.30 and 4.31).
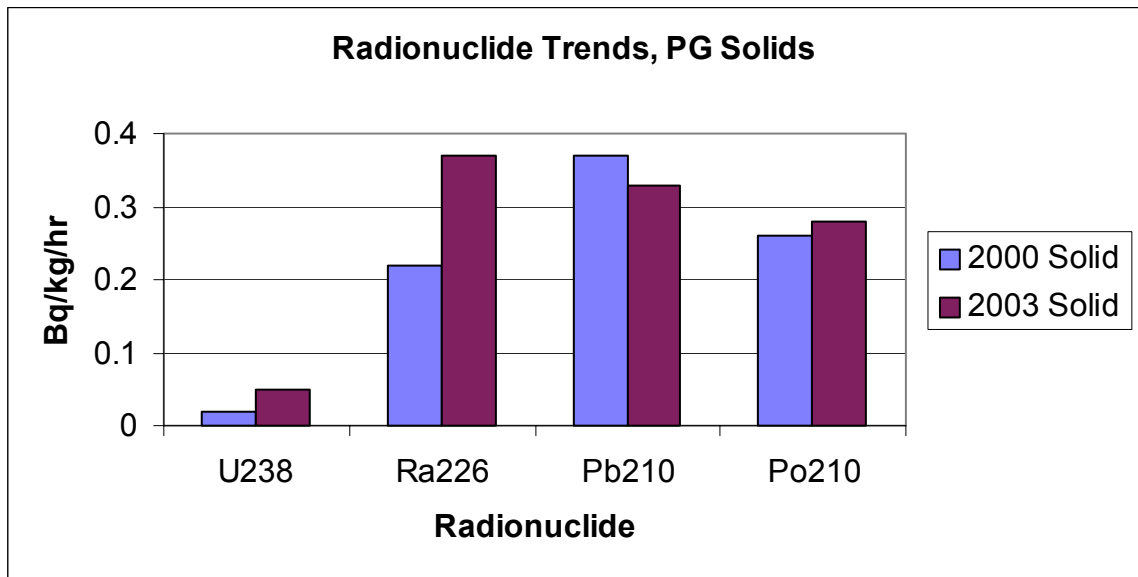

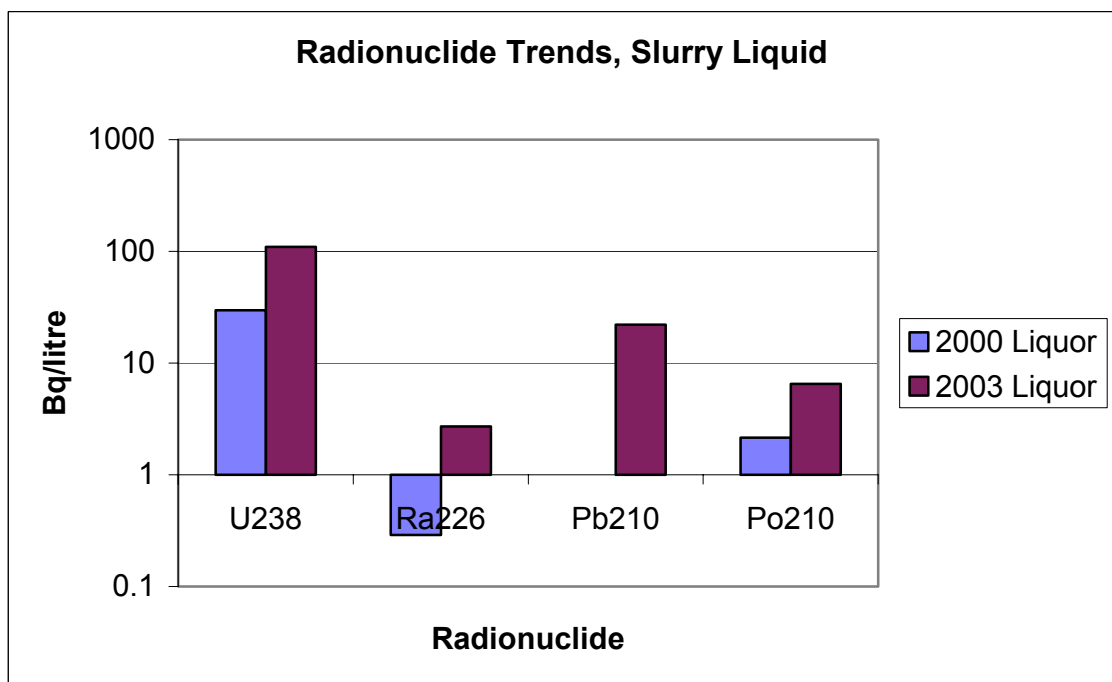**Figure 4.30   Radionuclide trends, PG slurry solid phase.**

Figure 4.31   Radionuclide trends, PG slurry liquid phase.

This is believed to be the result of the continuous recirculation of acid process water from the plant, through the re-slurry system to the stack, drained from the stack and returned to the re-slurry tank, as radionuclides are known to concentrate under these conditions (Brown 2003 *pers. comm.*).

4.8   SUMMARY

The sampling program undertaken in this study has produced a range of base-line results about the Phosphate Hill PG that were previously unknown. This includes the full details of the major and trace element composition and crystal morphology of the hemihydrate gypsum filtercake from the phosphoric acid plant, the newly formed dihydrate gypsum deposited on the stack from the re-slurry tank and older dihydrate gypsum that has been held on the stack for some time. The study has confirmed that, although the chemistry and morphology of the gypsum contained within the PG is much the same as that produced in similar plants throughout the world (see Tables 5.1 and 5.2), the final composition of the product is different. This specifically relates to the high amount of silica contained within the mix, which is a direct reflection of the amount of silicate impurities contained within the parent ore.

Gangue minerals identified in the PG in this study have also identified the presence of species that can only have been derived from the parent ore but which have been previously unidentified in that source. A member of the rare ettringite group has also been identified. These minerals are discussed in detail in section 5.

The study has also identified the composition of the recycled acid process water used in the re-slurrying process. This part of the gypsum conversion and transport system has not previously been the subject of in-depth examination.   The finding of most importance in this area is the increase in radionuclide content in the liquid component of the PG slurry, which seems to stem from the recycling of the fluid. This result was unexpected and may require ongoing monitoring in the future, while disposal options for contaminated liquid may need to be considered.

The final part of the process has identified for the first time the chemical composition of leachate derived from water input into the three specific types of PG found on site (hemihydrate filtercake, newly formed dihydrate from the re-slurry tank and aged dihydrate from the stack). The study has not only studied the changing composition of leachate derived from different types of PG over several inundation events but also the changes to the chemical composition of the specified PG types. The latter in particular was an area that was unknown before this study. The results should thus be of major importance to the Company in planning the long-term closure strategies for the existing stacks and for determining what methods of PG storage will be used in the long-term.